



**HAL**  
open science

# Storm response and multi-annual recovery of eight coastal dunes spread along the Atlantic coast of Europe

Olivier Burvingt, Bruno Castelle

## ► To cite this version:

Olivier Burvingt, Bruno Castelle. Storm response and multi-annual recovery of eight coastal dunes spread along the Atlantic coast of Europe. *Geomorphology*, 2023, 435, pp.108735. 10.1016/j.geomorph.2023.108735 . hal-04266562

**HAL Id: hal-04266562**

**<https://hal.science/hal-04266562>**

Submitted on 31 Oct 2023

**HAL** is a multi-disciplinary open access archive for the deposit and dissemination of scientific research documents, whether they are published or not. The documents may come from teaching and research institutions in France or abroad, or from public or private research centers.

L'archive ouverte pluridisciplinaire **HAL**, est destinée au dépôt et à la diffusion de documents scientifiques de niveau recherche, publiés ou non, émanant des établissements d'enseignement et de recherche français ou étrangers, des laboratoires publics ou privés.

# Storm response and multi-annual recovery of eight coastal dunes spread along the Atlantic coast of Europe

Olivier Burvingt<sup>1</sup>, Bruno Castelle<sup>1</sup>.

1. Univ. Bordeaux, CNRS, Bordeaux INP, EPOC, UMR 5805, F-33600 Pessac, France

## Highlights

- The 2013/14 winter was a major erosive event at eight European coastal dunes
- Coastal dunes with steeper pre-storm slopes lost the largest sand volumes
- Alongshore variable storm response is controlled by pre-storm dune topography
- Percentage of recovery is well correlated to local chronic shoreline change rate
- Dune crest elevation increase rate exceeds sea level rise rate at all sites

## Keywords

Coastal dunes; storm; recovery; airborne LiDAR; sea level rise

## Abstract

Coastal dunes are natural barriers against coastal flooding, and represent large sources of sediment to mitigate coastal erosion, besides being a natural habitat for many living beings. Yet, these complex environments are threatened by sea level rise and possibly enhanced storminess. Most of the studies on coastal dune erosion and recovery from storms are either site specific or focus on a short-time scale, from months to a couple of years. Here, airborne LiDAR data collected from 2011 to 2020 at eight diverse coastal dunes, spread from NW England to SW France, were analysed to study their response, and recovery from the most energetic extreme storms wave conditions since at least 1948.

Results show that the 2013/14 winter was the first or second largest erosive event (from -14 to -290 m<sup>3</sup>/m dune volume loss) from 2011 to 2020 at all sites. The magnitude of storm-driven sand volume loss was mainly controlled by dune face slope ( $r = 0.84$ ). Dunes with steeper pre-storm slopes lost the largest volumes of sand. At a dune scale, the scarping height was also well correlated to the dune face slope at sites where storm response was characterized by limited alongshore variability. Dune recovery was site specific (no recovery, partial, complete, excess), with dunes that either progressively returned to their pre-storm morphology or were reshaped while recovering. Percentage of dune sand volume recovery was well correlated to the local and long-term satellite-derived shoreline change rate computed from 1984 to 2021 ( $r = 0.81$ ), suggesting that dune recovery is mainly controlled by the local coastal sediment budget. The rate of dune crest elevation increase (from 4.2 to 12 cm/year) at four of the study sites from 2011 to 2020, largely exceeded sea level rise rate over the past decade ( $3.3 \pm 0.7$  mm/year). These results provide key insight into the contrasting resilience of some of the most exposed coastal dunes along the Atlantic coast that recover at different rates following the same sequence of extreme storms.

## **1. Introduction**

Coastal dunes are exposed and complex environments shaped by multiple interactions between waves, wind and vegetation (Delgado-Fernandez and Davidson-Arnott, 2011; De Vries et al., 2012; Hesp et al., 2013; Ruessink et al., 2019; Bauer et al., 2022), with morphological changes from centimetres to kilometres scale (Walker et al., 2017). Airborne light detection and ranging (LiDAR) data offers the opportunity to study morphological changes on a regional scale and in a non-invasive way (Burvingt et al., 2017; Nicolae-Lerma et al., 2019; Konstantinou et al., 2021), with a horizontal resolution  $< 1$  m and a vertical accuracy of c.  $\pm 15$  cm (Sallenger et al., 2001; Nicolae-Lerma et al., 2022). The largest coastal dune morphological changes are generally observed when storm waves coincide with high water levels (Masselink et al., 2015). The extreme storm wave conditions in the northeast

Atlantic during the 2013/14 winter are considered as the most energetic since at least 1948 (Masselink et al., 2016) and caused severe beach and dune erosion all along the Atlantic coast of Europe (Blaise et al., 2015; Castelle et al., 2015; Dissanayake et al., 2015; Masselink et al., 2015; Autret et al., 2016; Pye and Blott, 2016). The storm response of coastal dunes was shown to be controlled by wave characteristics at the coast (Castelle et al., 2015), surge levels (Pye and Blott, 2016), the degree of exposure to the storm waves (Burvingt et al., 2017) and the storm clustering effect (Dissanayake et al., 2015). Previous work worldwide showed that the alongshore variability in coastal dune response to extreme storms is controlled by morphological or geological characteristics such as the pre-storm alongshore variability of dune morphology (Houser, 2013; Cohn et al., 2021), the pre-storm offshore sandbar morphology (Castelle et al., 2015), the degree to which the beach is embayed (Burvingt et al., 2017).

Studying the period of recovery following extreme storms informs about the resilience of coastal areas. Beach recovery processes on cross-shore dominated beaches occur over a wide range of timescales: from years to decades (Splinter et al., 2011; Houser et al., 2015; Scott et al., 2016; Castelle et al., 2017a; Phillips et al., 2017; Burvingt et al., 2018; Robin et al., 2020; Konstantinou et al., 2021; Masselink et al., 2022). Although beach recovery is mainly controlled by the incident wave energy over the subsequent months or years (Burvingt et al., 2018), it also relies on the interactions between the beach and the intertidal/subtidal bar (Aagard et al., 2004; Scott et al., 2016; Brooks et al., 2017; Phillips et al., 2017) and/or subaerial dune systems (Suanez et al., 2012; Houser et al., 2015). The magnitude of the storm response can also play an important role in the recovery time of beaches (Konstantinou et al., 2021).

Transgression distances due to sea level rise were shown to be small in comparison to characteristic shoreline excursions driven by storm events and subsequent reconstruction phases (Davidson-Arnott and Bauer, 2021). Extreme storms can also have a positive contribution to the nearshore sediment budget and potentially mitigate adverse SLR impacts (Harley et al., 2022). In light of this findings, the

analysis of the response and recovery from extreme storms at various dune sites can inform on the resilience of coastal dunes in a context of sea level rise and possibly enhanced storminess.

The airborne LiDAR data acquired through different coastal monitoring programs along the Atlantic coast of Europe over the last decade, offers the unique opportunity to compare coastal dune response over the same period of time and using the same approach, at sites with diverse morphological and hydrodynamic settings. The eight coastal dunes were selected for their similar exposure to storm waves, but they show a high diversity in morphological characteristics (e.g. height, size, beach state, etc...). While several and mostly site-specific studies focused on the controlling factors of dune response to storms, very few studies examined the recovery of coastal dunes from extreme storms at large spatial and multi-annual scales. The main objective of this study is therefore to examine multi-annual dune change in a context of extreme storms at eight study sites from NW England to SW France. First, the cross-shore and alongshore storm-driven dune responses are presented and analysed to determine their controlling factors. The second objective is to quantify the degree of recovery for these eight coastal dunes over the six years following the extreme winter, and to explain its differences by analysing its controlling factors. Conclusions on the resilience of these coastal dunes are also made based on the characteristics, the duration and magnitude of their recovery.

## **2. Study area, Datasets and Methods**

### **2.1. Study area**

The eight coastal dune sites are spread along the Atlantic coast of Europe, from NW England to SW France (Fig. 1). These sites were selected for their exposure to storm waves generated in the north Atlantic Ocean, and the availability of large scale and multi-annual topographic datasets. These eight study sites are characterised by different environmental settings (Table 1) such as climate, waves,

tides, winds, geology, etc., resulting in a large variability of coastal dunes in terms of morphology (height, size, shape), beach type (open or embayed), vegetation cover (size, density) and anthropogenic pressure. Although they are all exposed to similar wave climates, the degree of exposure to storm wave events varies due to their location and orientation. A relatively wide range of tidal regimes can also be found, from macrotidal (NW England) to mesotidal (SW France).



Figure 1. Location map and photos of the eight study sites with from north to south: Formby (FBY), Penhale (PNH), Gwithian (GWI), Notre-Dame-de-Monts (NDM), Carcans (CAR), Lacanau (LAC), Truc Vert (TCV), and Lette Blanche (LBL).

Table 1. Range of dune height, dune width, dune length, beach state, lower dune elevation threshold ( $Z_0$ according to the Ordnance Datum Newlyn for the English sites and according to the NGF - IGN69 datum for French sites), dune orientation ( $\alpha$ ), and mean spring tidal range (m).							
	<b>Dune height (m)</b>	<b>Dune width (m)</b>	<b>Dune length (km)</b>	<b>Beach state</b>	<b><math>Z_0</math> (m)</b>	<b><math>\alpha</math> (°)</b>	<b>MSTR (m)</b>
Formby (FBY)	[6 - 16]	150	1600	Open	4 (ODN)	287	8
Penhale (PNH)	[30 - 60]	200	2200	Semi-embayed	2.5 (ODN)	283	6.3
Gwithian (GWI)	[12 - 50]	300	3400	Semi-embayed	2.5 (ODN)	315	6.3
Notre-Dame-des-Monts (NDM)	[5 - 15]	150	700	Open	2.5 (NGF)	260	4
Carcans (CAR)	[15 - 25]	200	4000	Open	2.5 (NGF)	275	3.7
Lacanau (LAC)	[12 - 28]	250	4000	Open	2.5 (NGF)	275	3.7
Truc Vert (TCV)	[15 - 24]	325	4000	Open	2.5 (NGF)	278	3.7

Lette Blanche (LBL)	[13 - 25]	280	4000	Open	2.5 (NGF)	282	3.7
---------------------	-----------	-----	------	------	--------------	-----	-----

The majority of wave events affecting the European Atlantic coast are generated by extratropical storms developing within the mid-latitude westerly wind belt (Lozano et al., 2004). Storminess in the north Atlantic due to extra-tropical storms is strongly linked to the North Atlantic Oscillation (NAO) and the West Europe Pressure Anomaly (WEPA), which are characterized by considerable inter-annual and inter-decadal variability (Castelle et al., 2017b) affecting coastal response (Dodet et al., 2019). The 2013/14 winter was characterized by a positive winter NAO and the largest WEPA index on record, causing extreme wave conditions across all study sites.

## 2.2. Study sites

### 2.2.1. Formby, NW England (FBY)

Formby (FBY) dune is located along the Sefton coast (Merseyside, NW England). This open coast is mainly exposed to W-NW waves originating from the Irish Sea, and is also influenced by estuarine regimes, the Ribble and Mersey estuaries being located 20 km up north and 10 km down south to Formby, respectively (Pye and Blott, 2016). Significant wave heights only exceed 4 m during major wave events (Brown et al., 2010). The tidal regime is semi-diurnal and macrotidal, with a mean spring tidal range (MSTR) of approximately 8 m, exposing a wide intertidal zone at low tide characterized by large ridges. The stretch of dune selected here is 1.6 km long and 150 m wide, its height ranges from 6 to 16 m (Fig. 2). Dune vegetation is dominated by dense marram grass (Fig. 1). Formby dune also plays a major role in the protection against coastal flooding for the low-lying land of north Merseyside and west Lancashire (Pye and Blott, 2016).

### 2.2.2. Penhale (PNH) and Gwithian (GWI), SW England

The Cornish coast (SW England) offers a large number of diverse beaches (Scott et al., 2011). Amongst them, Penhale (PNH) and Gwithian (GWI) on the north coast of Cornwall are long and wide embayed sandy beaches backed by extensive dunes. They are exposed to regular North Atlantic swells, with an annual average significant wave height of 1.6 m and peak period of 10–11 s (Valiente et al., 2019). The tidal regime is semi-diurnal and macrotidal with a mean spring tidal range of 6.3 m (Poate et al., 2009). Penhale is a wide and dissipative beach embayed by prominent headlands (low tide embayment), while Gwithian beach is located in a shallow crescentic bay (St Ives Bay) with a wide and flat shoreface (Valiente et al., 2019). Both beaches and dunes are W-NW oriented and are exposed to the dominant wave approach. The stretch of dunes at Penhale and Gwithian selected here are 2.2 and 3.4 km long, 200 and 300 m wide, respectively. Their height ranges from 30 to 60 m, and from 12 to 50 m (Fig. 2). As with Formby dune, the vegetation is dominated by dense marram grass (Fig. 1).

#### 2.2.3. Notre-Dame-de-Monts (NDM), NW France

Located between the rocky shores of Brittany and the Aquitanian open sandy coast, the Vendée coast (NW France) is characterized by long and open or embayed sandy beaches (Le Mauff et al., 2018). Bergère beach is a wide, dissipative and open beach located north to Notre-Dame-de-Monts (NDM). A two-year wave-buoy record collected offshore of this beach showed a mean significant wave height of 1.81 m, and a mean period of 5.89 s (Butel et al., 2002). The tidal regime is semi-diurnal and macrotidal with a mean spring tidal range of 4 m. Bergère is W orientated and is well exposed to the dominant W-WNW and WSW-W wave incidence (Butel et al., 2002). The stretch of dune selected here is 700 m long, 150 m wide, and its height ranges from 5 to 15 m (Fig. 2). Dune vegetation is dominated by sparse marram grass and the dune is backed by a large forest mainly comprised of maritime pines (Fig. 1).

#### 2.2.4. Carcans (CAR), Lacanau (LAC), Truc Vert (TCV) and Lette Blanche (LBL), SW France

The open sandy coast of Aquitaine (SW France) is 230 km long and extends from the Gironde estuary to the Adour estuary. It is exposed to North Atlantic swells with a dominant W to NW incidence (Butel

et al., 2002), and mean significant wave height ranges from 1.1 m in July to 2.4 m in January, while mean peak wave period ranges from 8.5 s in July and 13 s in January (Castelle et al., 2017a). Almost the entire coast is characterised by a net southerly longshore drift of the order of  $100\text{--}650 \cdot 10^3 \text{ m}^3/\text{year}$ . The tidal regime is semi-diurnal and meso- to macrotidal, with a mean spring tidal range of 3.7 m. This coast is also characterised by intermediate and double barred beaches, with an inner intertidal bar that commonly have a transverse bar and rip channel morphology. The outer subtidal bar is generally well-developed and often exhibits crescentic patterns with a relatively regular spacing of approximately 600–800 m (Castelle et al., 2007; Almar et al., 2009). All beaches are backed by a large coastal dune field (Bossard and Nicolae Lerma, 2020), which size and shape is inherited by both natural processes and 162 years of human interventions (Robin et al., 2021). The stretch of dunes at Carcans (CAR), Lacanau (LAC), Truc Vert (TCV) and Lette Blanche (LBL) are all 4 km long, and respectively 200, 250, 325 and 280 m wide (Fig. 2). Their heights vary from 15 to 25 m (CAR), from 12 to 28 m (LAC), from 15 to 24 m (TCV), and from 13 to 25 m (LBL). As with Notre-Dame-de-Monts, dune vegetation is dominated by sparse marram grass and the dunes is backed by large forests mainly comprised of maritime pines (Fig. 1).

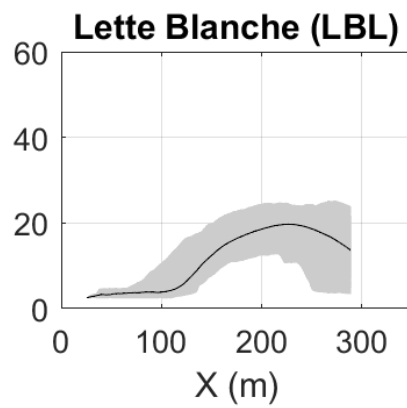
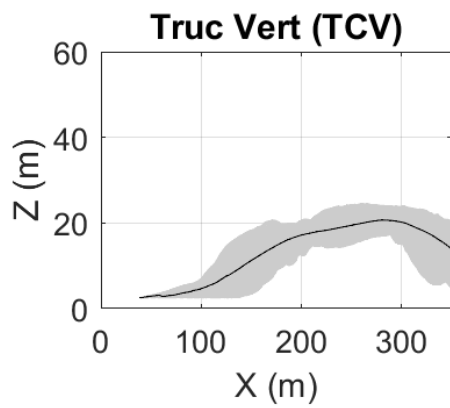
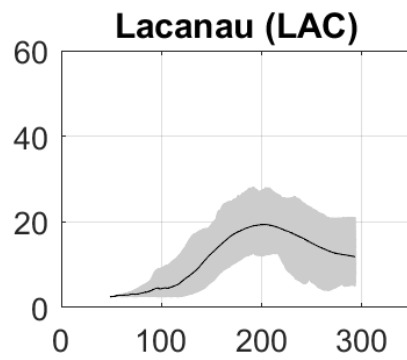
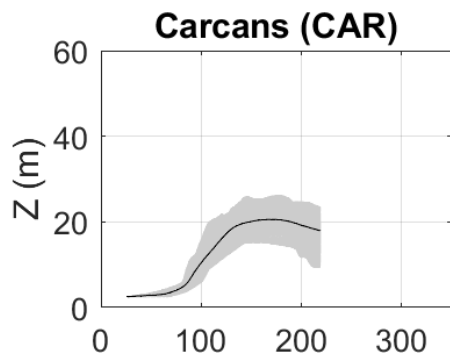
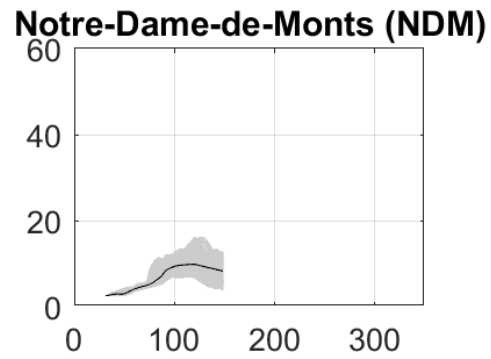
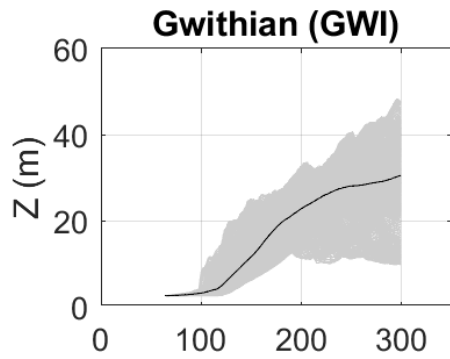
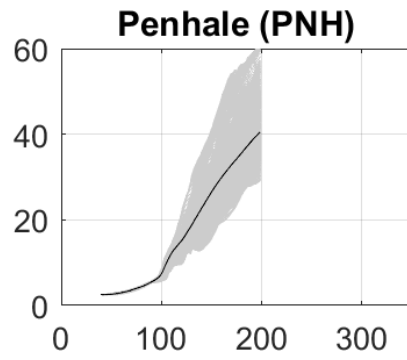
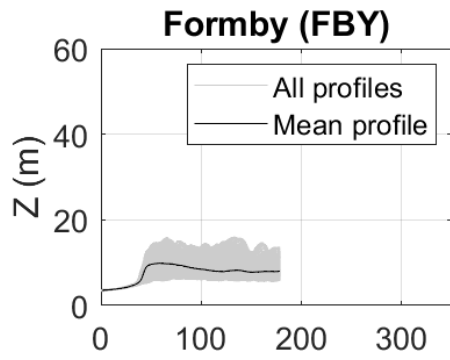


Figure 2. Alongshore-averaged dune profile (thick black) superimposed onto all cross-shore profiles (light grey) extracted from the pre-2014 airborne LiDAR survey showing the diversity of size and shape of the coastal dunes and their alongshore variability.

## 2.3. Datasets

### 2.3.1. Lidar datasets

Airborne LiDAR Digital Elevation Models (DEMs) are valuable tools to study coastal morphological change (Burvingt et al., 2017; Nicolae Lerma et al., 2022), with several airborne LiDAR datasets from 2011 to 2020 available for our eight study sites (Table 2). Since LiDAR campaigns have not been carried out in 2013 at only one site (FBY), the timing of the 'pre-2013/14 winter storm' datasets can be an issue. The most recent pre-2013/14 winter surveys were either carried out in 2011, 2012 or 2013 (Table 2), while all post-storm surveys were acquired in 2014 except for the NDM post-storm survey which was carried out in 2015. This makes attributing the difference in morphology to the 2013/14 storms debatable. However, many studies demonstrated that the morphological changes caused by the 2013/14 winter were typically much larger than the changes observed during the previous years (Masselink et al., 2015; Castelle et al., 2015; Scott et al., 2016; Burvingt et al., 2018; Konstantinou et al 2021). The morphological changes derived from the LiDAR data between 2011 and 2014, or between 2012 and 2014 are therefore considered to represent the changes that occurred during the 2013/14 winter. Airborne LiDAR datasets collected along the coastline of NW and SW England (FBY, PNH and GWI) are reported to have a vertical accuracy of less than +/-15 cm, while the vertical accuracy of the LiDAR datasets collected at NDM and along SW France are 8 cm (Launeau et al., 2018) and from 10 to 20 cm (Nicolae-Lerma et al., 2019), respectively. All LiDAR datasets were interpolated to produce topographic DEMs on a local 1 m x 1 m regular grid. LiDAR surveys were performed either during spring

and autumn. Given the strong seasonal variability of beach state and volume (Masselink et al., 2015; Castelle et al., 2015; Pye and Blott, 2016, Le Mauff et al., 2018), the beach system was discarded from the analysis in order to avoid seasonal noise.

### 2.3.2 Morphological change parameters

The DEMs derived from LiDAR datasets offer the opportunity to define several parameters to assess the morphological changes observed on the difference of DEMs (DoDs) from 2011 to 2020 (Fig. 3). Some parameters such as volume change per width  $dV$  ( $m^3/m$ ) can be computed and averaged alongshore over the entire DEM ( $\overline{dV}$ , with the  $(\cdot)$  notation denoting alongshore averaging). Other parameters such as the cross-shore dune foot position  $X_{foot}$  and height  $Z_{foot}$ , or dune crest height  $Z_{crest}$  can be hardly identified automatically due to the large alongshore variability in dune morphology. These parameters, in addition to the post-storm dune scarping height,  $Z_{scarp}$ , were manually computed over 40 regularly-spaced profiles for each study site (Fig. 3), and averaged to provide the corresponding alongshore-averaged time-series (Fig. 4). Following the work published by Wernette et al. (2018), dune foot was defined as the location marked by an increase in slope moving landward from the shoreline. Here, for all study sites, the post-storm (2014) scarped profiles were considered as the most appropriate profiles to determine dune foot elevation. The same authors also defined the dune crest as a local relative topographic maximum, marked by a significant decrease in slope gradient. Here, using the maximum elevation of the dune or the point where there is a decrease in slope gradient would not, or only partially describe the morphological changes which were observed on the upper part of the dune at most of the profiles. Instead, all surveys of each profile were plotted together, and a cross-shore position along the dune profile where dune elevation changes are representative of the entire upper part of the dune for the whole study period was selected. Although this definition is subjective and make the results not comparable with other studies, this parameter was found to give a better description on how dune elevation changed from 2011 to 2020, and lead to a robust

comparison between our study sites. Dune face slopes were thus not calculated using  $Z_{\text{crest}}$  but using  $Z_{\text{scarp}}$ , the latter giving a better estimate of the dune face slope.

These parameters were also used to vertically divide dune profiles into classes and define the corresponding volumes of sand. For this study, the volume comprised between the start of the dune profile  $Z_0$  (Table 1) and the dune foot was defined as  $V_{\text{foot}}$  ( $\text{m}^3/\text{m}$ ), the volume comprised between the dune foot and the dune crest was defined as  $V_{\text{face}}$  ( $\text{m}^3/\text{m}$ ), and the volume comprised between the dune crest and the end of the dune profile was defined as  $V_{\text{top}}$  ( $\text{m}^3/\text{m}$ ). The alongshore-averaged percentage of recovery,  $\overline{P_{\text{recovery}}}$  (%), that corresponds to the ratio of the volume recovered between 2014 and 2020 in comparison to the volumes lost during the pre-2014 and the 2014 surveys and is expressed in percentage, was also calculated for each study site.

Long-term (38 years) shoreline change rates were also computed to explore how such long-term trend, and thus local coastal sediment budget, controls the timing and magnitude of coastal dune erosion and recovery. The CoastSat toolkit (Vos et al., 2019) was used to extract waterlines from publicly available optical satellite data from 1984 to 2021 through Google Earth Engine, namely Landsat 5, 7 & 8 (L5, L7, L8, 30-m spatial resolution) and Sentinel-2 (S2, 10-m spatial resolution) satellite images without any water level correction following Castelle et al. (2022). The 38-year time series of shoreline positions, including between 97 (GWI) and 678 (NDM) data, was linearly regressed to estimate the alongshore-averaged long-term shoreline changes,  $R$  (m/year), at each of the eight sites (Table 2).

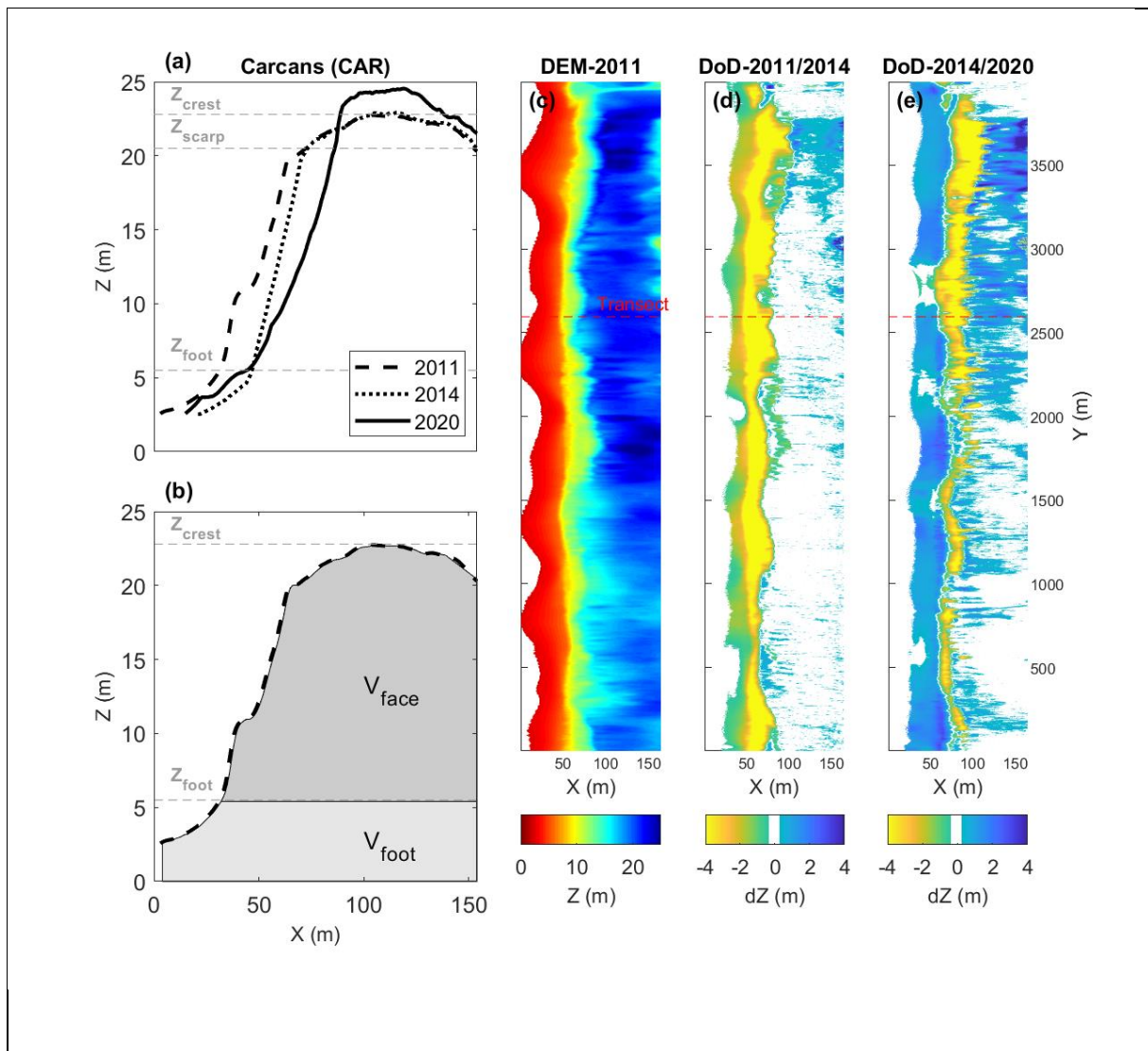


Figure 3. (a) Representative cross-shore profiles at Carcans showing the manually detected parameters used to describe morphological changes: the dune crest height,  $Z_{crest}$ , the post-storm scarping height,  $Z_{scarp}$ , and the dune foot height,  $Z_{foot}$ . (b) Dune profile showing the vertical division of the sand volumes:  $V_{foot}$  corresponding to the volume from the start of the dune profile to the dune foot,  $V_{face}$  corresponding to the volume comprised between the dune foot and the dune crest and,  $V_{top}$  corresponding to the volume comprised between the dune crest and the end of the dune profile. (c, d and e) Examples of digital Elevation Model (DEM) and difference of DEMs (DoD) used to derive alongshore averaged parameters.

Table 2. Airborne LiDAR datasets with vertical accuracies and the satellite-derived and alongshore-averaged long-term shoreline change rates,  $R$  (m/year), for the eight study sites.

Study sites	LiDAR datasets	LiDAR data vertical accuracy (cm)	$R$ (m/year)
Formby (FBY)	2013, 2014, 2016, 2017, 2018, 2020	$\pm 15$ (data.gov.uk)	-2.1
Penhale (PNH)	2012, 2014, 2016, 2017, 2018, 2020	$\pm 15$ (Wiggins et al., 2019a)	- 0.1
Gwithian (GWI)	2012, 2014, 2016, 2017, 2019, 2020	$\pm 15$ (Wiggins et al., 2019a)	0.4
Notre-Dame-des-Monts (NDM)	2013, 2015, 2017, 2018, 2019, 2020	8 (Launeau et al., 2018)	0.2
Carcans (CAR)	2011, 2014, 2016, 2017, 2018, 2019, 2020	[10 - 20] (Nicolae Lerma et al., 2019)	-0.6
Lacanau (LAC)	2011, 2014, 2016, 2017, 2018, 2019, 2020	[10 - 20] (Nicolae Lerma et al., 2019)	-0.3
Truc Vert (TCV)	2011, 2014, 2016, 2017, 2018, 2019, 2020	[10 - 20] (Nicolae Lerma et al., 2019)	0.3
Lette Blanche (LBL)	2011, 2014, 2016, 2017, 2018, 2019, 2020	[10 - 20] (Nicolae Lerma et al., 2019)	0

### 3. Results

#### 3.1. Multi-annual morphological changes

Time-series of the alongshore-averaged volume change per meter width,  $\overline{dV}$ , cross-shore dune foot position,  $\overline{dX_{foot}}$ , and dune crest height,  $\overline{dZ_{crest}}$ , were used to describe the morphological changes observed from 2011 to 2020 at the eight study sites (Fig. 4). For most of the study sites, these time-series show a short and large erosive period followed by a multi-annual recovery period. The 2013/14 winter represents the largest or second largest (FBY and LBL) loss of sand volumes (from -14 to -290 m<sup>3</sup>/m) for the eight study sites from 2011 to 2020 (Fig. 4a and 4b). This winter also caused the largest or second largest dune foot retreats (from -1.5 to -17 m) over the same period (Fig. 4c and 4d). Time-series of the dune crest height also shows that, in average, all dunes rose by tens of centimeters (from 0 to 70 cm) during the 2013/14 winter, except FBY (-0.31 cm) (Fig. 4e and 4f). Following this erosive winter, the eight study sites can be divided into three groups considering their recovery rates. Only three years after the 2013/14 winter, recovered volumes of sand at NDM, TCV and LBL exceeded the volumes that were lost during the 2013/14 winter. Despite a subsequent erosive winter (2018/2019), these dunes have larger or similar volumes of sand compare to the pre-2014 ones (+25, +90 and +16.5 m<sup>3</sup>/m respectively). In the second group, PNH, GWI, CAR, LAC show only very limited or limited volume recovery (12%, 63%, 11% and 36% respectively). For each of these four study sites, relatively large amounts of sand were recovered within the three years following the 2013/14 winter, as did the dunes of the first group. However, a large part of these recovered volumes were subsequently lost between 2018 and 2019 (CAR, LAC) or between 2018 and 2020 (PNH). The third group only comprises the dune of FBY that shows no recovery over the 6 years following the 2013/14 winter (Fig. 4a), its volume remained stable between 2014 and 2017, while a large volume of sand (-85 m<sup>3</sup>/m) was lost between 2018 and 2020. Similar patterns of erosion and recovery can be observed between the volume changes

and the dune foot positions at most of the study sites (FBY, PNH, GWI, NDM, TCV and LBL). However, the return of the dune foot position to its pre-2014 position at CAR and TCV dunes is much faster in comparison to the recovery of the volumes lost during the 2013/14 (Fig. 4d), indicating a change in dune morphology. The dune crest height changes at sites located in England and NDM do not any show clear trends as heights either increase or decrease throughout the years (Fig. 4e). Dune crest elevation changes are either large (>50 cm; FBY) or small (< 20 cm; PNH, GWI and NDM) at these four sites between 2011 and 2020. Along the Aquitaine coast (Fig. 4f), a relatively steady increase of the dune crest height can be observed at the four study sites between 2011 and 2020, by approximately 0.5 m (CAR and LBL) and 1 m (LAC and TCV).

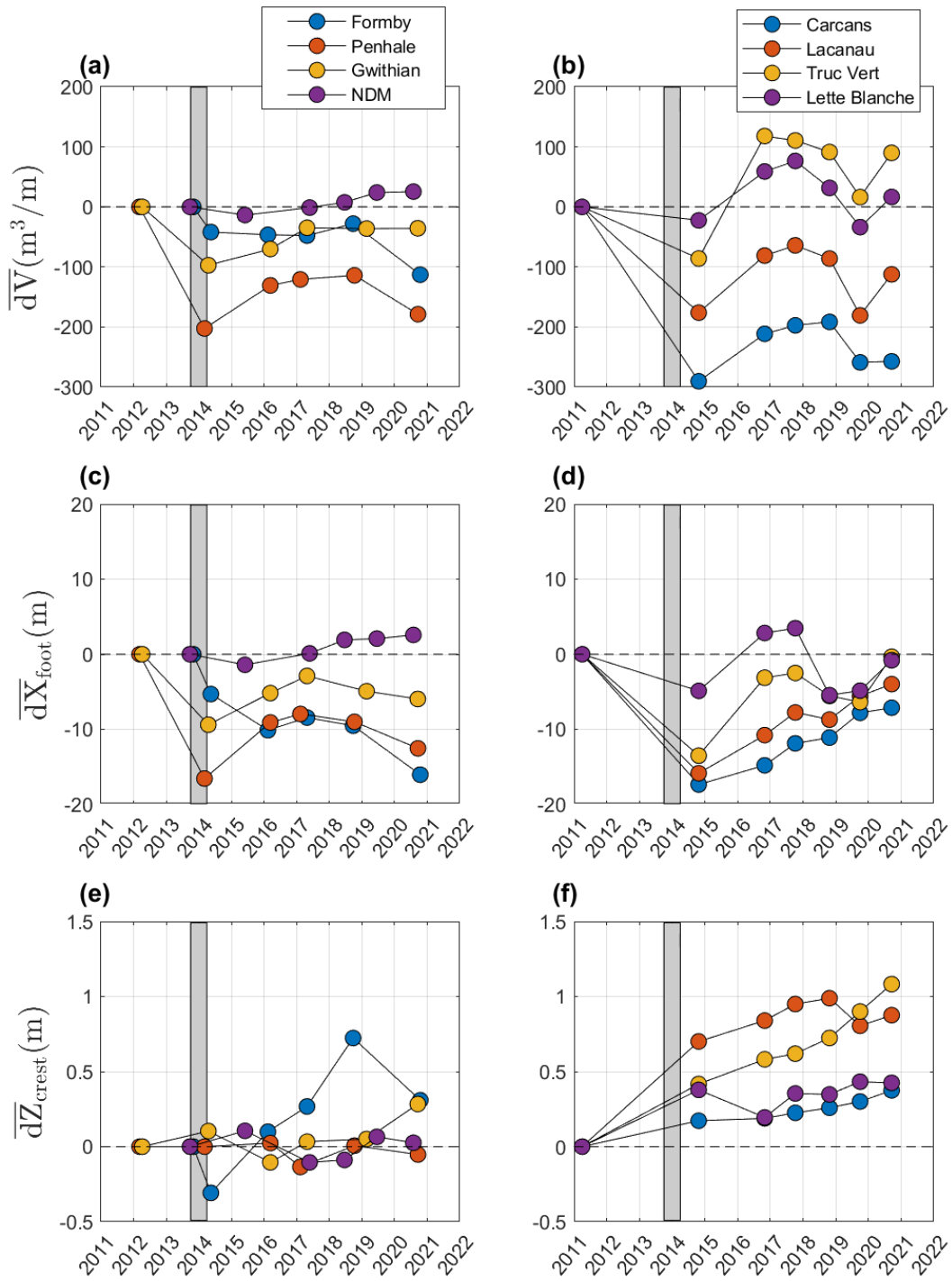


Figure 4. Time-series of the alongshore-averaged volume change per beach width  $\overline{dV}$ , dune foot position  $\overline{dX}_{\text{foot}}$ , and dune crest height  $\overline{dZ}_{\text{crest}}$  from 2011 to 2020 at the eight study sites.

The comparison of the alongshore-averaged volume changes ( $\overline{dV_{storm}}$ ) and dune foot position changes ( $\overline{dX_{storm}}$ ) over the 2013/14 winter show that the magnitude of the volumes lost during that winter is well correlated ( $r = 0.9$ ) to the magnitude of the dune foot retreat (Fig. 5a). A large correlation is also computed ( $r = 0.84$ ) when looking at the 2014-2020 recovery period (Fig. 5b). In both cases, no correlations were found between these parameters and the corresponding dune crest height changes,  $\overline{dZ_{storm}}$  and  $\overline{dZ_{recovery}}$ .

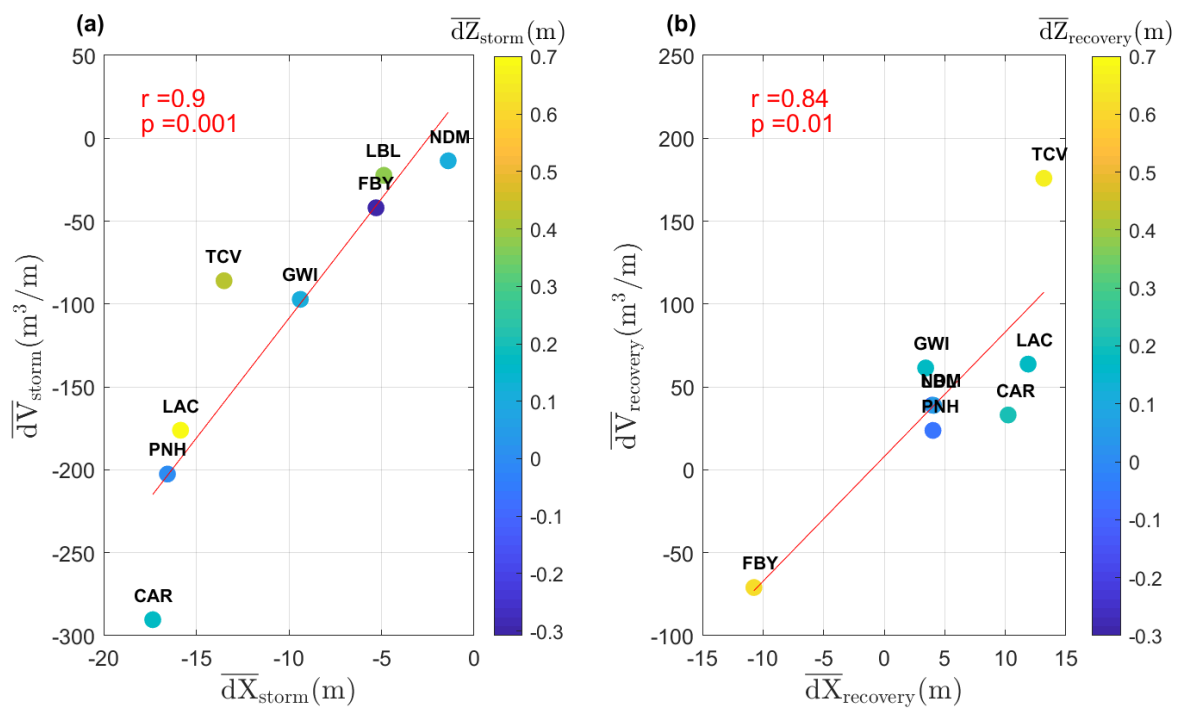


Figure 5. Alongshore-averaged volume changes over (a) the stormy period,  $\overline{dV_{storm}}$ , and (b) the recovery period,  $\overline{dV_{recovery}}$ , versus dune foot position changes,  $\overline{dX_{storm}}$  and  $\overline{dX_{recovery}}$ , and dune crest height changes,  $\overline{dZ_{storm}}$  and  $\overline{dZ_{recovery}}$ , over the same periods at the eight study sites. The Pearson correlation coefficient,  $r$ , and the p-value of the Wilcoxon Rank-Sum test are added to assess the statistical significance of these relationships.

## 3.2. Morphological response of coastal dunes to extreme storms

### 3.2.1. Dune profile response to extreme storms

Representative pre- and post-2014 cross-shore dune profiles were selected at the eight study sites to show and compare the dune profile response to extreme storms (Fig. 6). At relatively small dunes ( $\overline{Z_{crest}} < 15$  m), like FBY and NDM, two different responses were observed. At NDM, the dune morphology did not change substantially as the dune mostly translated landwards by a few meters (Fig. 6d), while the entire face of the dune, including the dune crest, was eroded at FBY causing a large retreat and a lowering of the dune crest (Fig. 6a). Noteworthy, the post-storm profile at NDM is likely to include a degree of recovery since LiDAR data were collected one year after the stormy period (2015). Dune scarping was observed at the six other dune sites causing a large retreat of the dune face, but no major morphological changes were observed behind the dune crest. Scarping heights,  $Z_{scarp}$ , are mostly comprised between 10 and 20 m at PNH (Fig. 6b) and GWI (Fig. 6c) with a weak alongshore variability, while moderate (CAR, Fig. 6e) and strong (LAC, TCV and LBL; Fig. 6f, 6g and 6h) alongshore variability were observed in SW France owing to the presence of megacusp embayments cutting the dune with a spacing of hundreds of meters (see Section 3.2.2). The increase in dune crest elevation observed at CAR, LAC, TCV and LBL and shown in Figure 4f does not appear in Figure 6 because of the scale of the figure, but positive vertical changes on the upper part of the dunes can be observed at LAC, for instance, in Fig.7d.

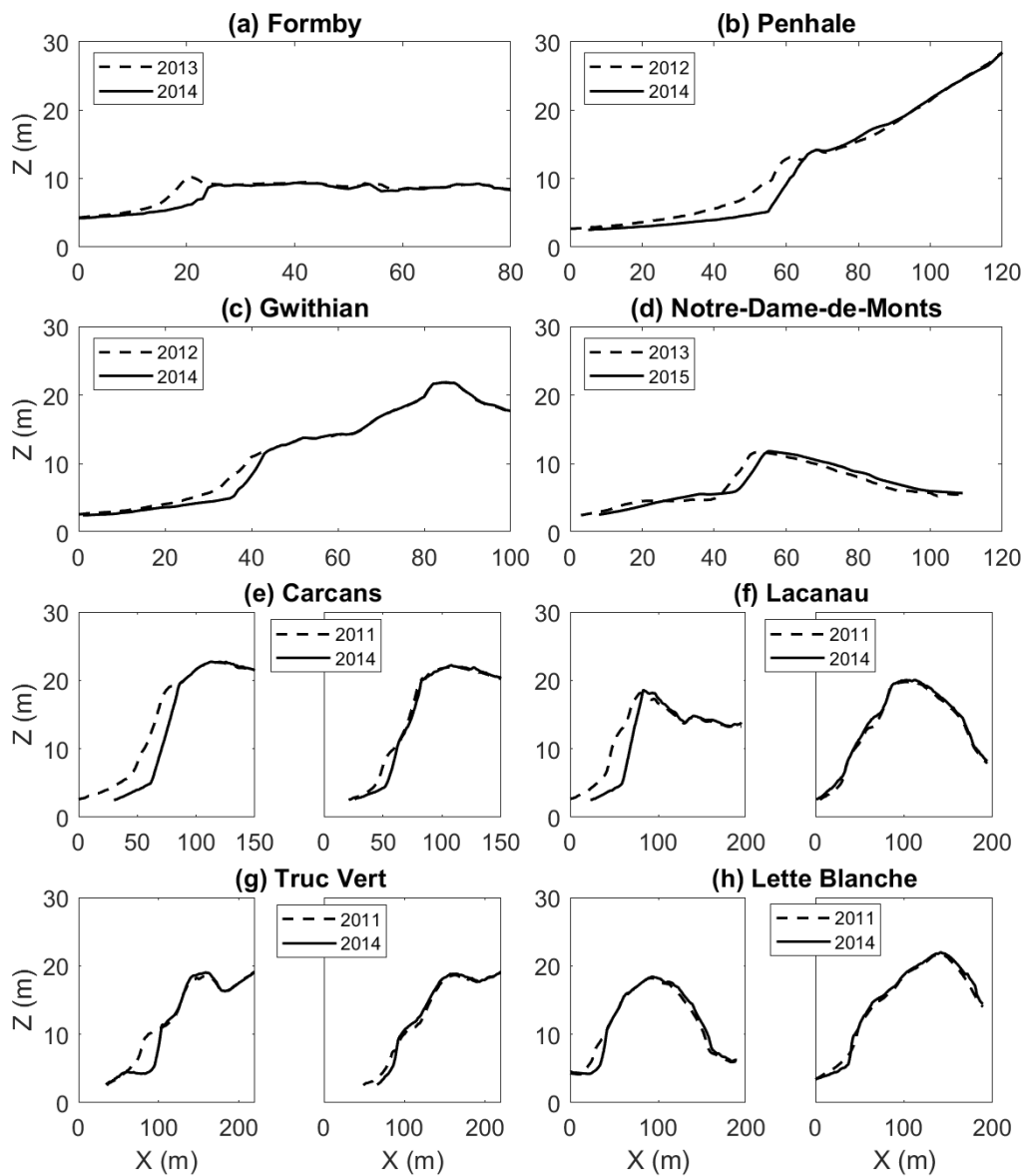


Figure 6. Representative pre- and post-2014 cross-shore dune profiles extracted from LiDAR data at the eight study sites.

### 3.2.2. Alongshore variability in dune response to extreme storms

The difference of pre-2014 and post-storm DEMs at PNH and LAC were used to show two contrasting examples of the morphological dune response to extreme storms (Fig. 7), where either limited (PNH) or strong (LAC) alongshore variability in storm response can be observed. The entire 1.5 km of dune front at PNH was subjected to severe and relatively alongshore-uniform erosion (Fig. 7b), while a series of severe erosion hotspots (megacusp embayments) alternate alongshore with a spacing of approximately 500 m at LAC (Fig. 7d).

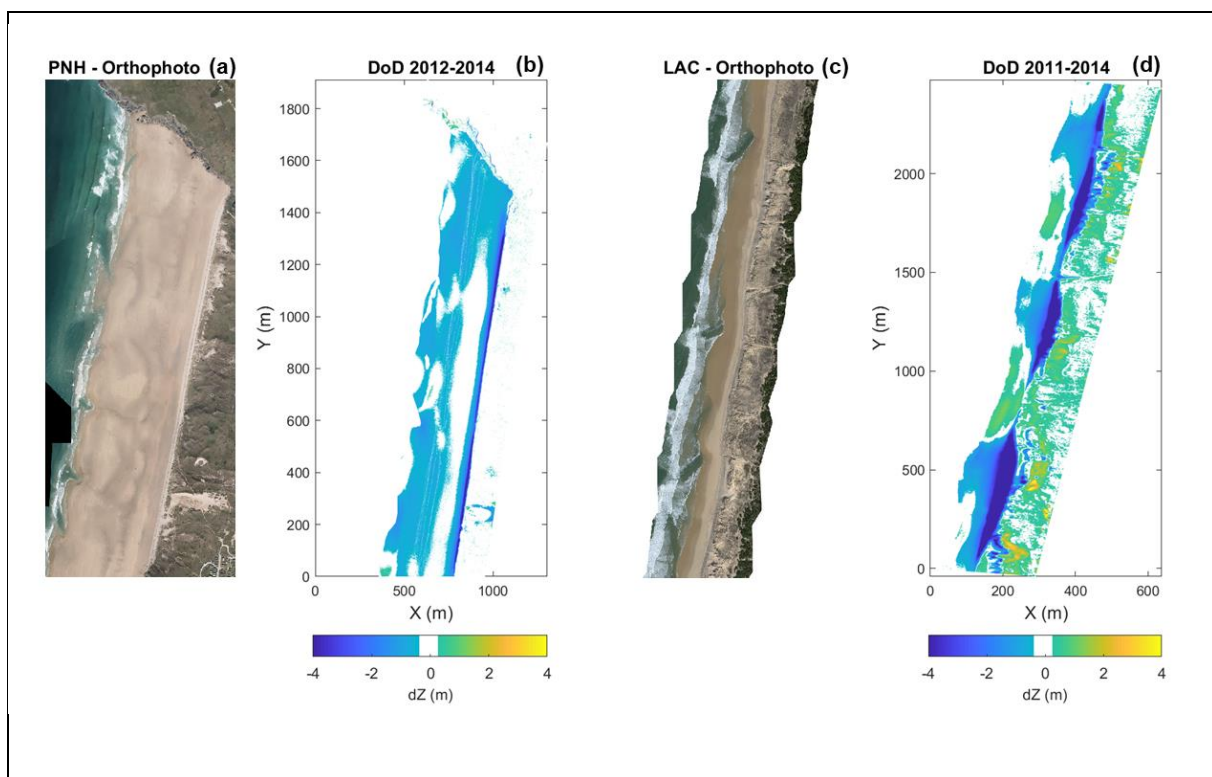


Figure 7. Orthophotos (a and c) and difference of pre- and post-2014 DEMs (b and d) showing two contrasting examples of storm responses at Penahle (PNH) and Lacanau (LAC), respectively.

A dimensionless index,  $LVI$ , proposed by Burvintg et al. (2017) was used to compare the longshore variability in storm response at the eight study sites (Table 2). This index is based on the alongshore-averaged volumetric change ( $\overline{dV_{storm}}$ ) and its standard deviation ( $\sigma_{dV_{storm}}$ ). It varies between 0 and 1 with higher values representing greater longshore variability in storm response. Based on this index,

two groups can be defined: a first group (FBY, PNH, GWI and CAR) where dunes show limited longshore variability in storm response with LVI values ranging from 0.19 to 0.36, and a second group (NDM, LAC, TCV and LBL) where dunes show a larger longshore variability in storm response, with LVI values ranging from 0.48 to 0.58 (Table 2).

Table 2. Longshore variability index, <i>LVI</i> , for each study site, and the corresponding absolute values of the alongshore-averaged volume changes $\overline{dV_{storm}}$ and its standard deviation, $\sigma_{dV_{storm}}$ .			
Sites	$ \overline{dV_{storm}} $ (m <sup>3</sup> /m)	$\sigma_{dV_{storm}}$	LVI
Formby	43	23	0.35
Penhale	203	46	0.19
Gwithian	97	34	0.26
Notre-Dame-de-Monts	19	17	0.48
Carcans	290	166	0.36
Lacanau	208	219	0.51
Truc Vert	109	117	0.52
Lette blanche	71	99	0.58

### 3.2.3. Controlling factor of dune response to extreme storms

Differences of slope were noticed between the different study sites. The alongshore-averaged dune slope,  $\overline{Slope}$ , was compared to the averaged volume of sand lost during the 2013/14 winter,  $\overline{dV_{storm}}$ , for each study site (Fig. 8a). Results show that the steeper the dune, the larger the loss of volume of sand was ( $r = -0.84$ ,  $p$ -value = 0.0002). At the six study sites where dune scarping was observed (PNH, GWI, CAR, LAC, TCV, LBL), results also show that the dune slope has a strong control on the scarping

height. A good correlation ( $r = 0.85$ ,  $p$ -value = 0.002) was found when comparing the alongshore-averaged dune slope,  $\overline{Slope}$ , and the alongshore-averaged dune scarping height,  $\overline{Z_{scarp}}$  (Fig 8b).

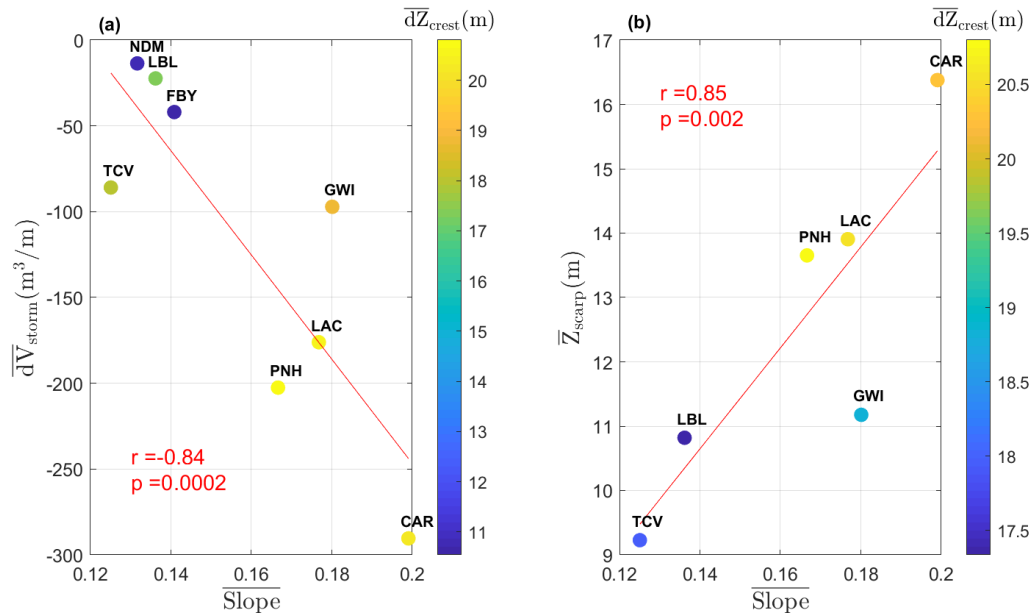


Figure 8. (a) Alongshore-averaged volume changes during the stormy period,  $\overline{dV_{storm}}$ , in comparison to the pre-2014 alongshore-averaged slope,  $\overline{Slope}$ , and dune crest height,  $\overline{dZ_{crest}}$ , at the eight study sites. (b) Alongshore-averaged dune scarping height,  $\overline{Z_{scarp}}$ , in comparison to the pre-2014 alongshore-averaged slope,  $\overline{Slope}$ , and dune crest height,  $\overline{dZ_{crest}}$ , at the six study sites where dune scarping was observed. The Pearson correlation coefficient,  $r$ , and the  $p$ -value of the Wilcoxon Rank-Sum test are added to assess the statistical significance of the relationship.

The post-storm dune scarping heights,  $Z_{scarp}$ , were also compared to the corresponding dune slopes,  $Slope$ , at 40 cross-shore profiles distributed along each of the study sites where dune scarping was observed (Fig. 9). Results show that the post-storm scarping height is strongly controlled by the pre-2014 dune slope at dunes with limited longshore variability in storm response ( $LVI < 0.26$ ) such as PNH

( $r = 0.86$ ) and GWI ( $r = 0.95$ ) (Fig. 9a and 9b), in comparison to smaller correlations ( $0.57 < r < 0.62$ ) that were found at sites with moderate ( $LVI = 0.36$ ) and large ( $LVI > 0.51$ ) longshore variability in dune response at CAR (Fig. 9c) and LAC, TCV and LBL (Fig. 9d, 9e and 9f), respectively.

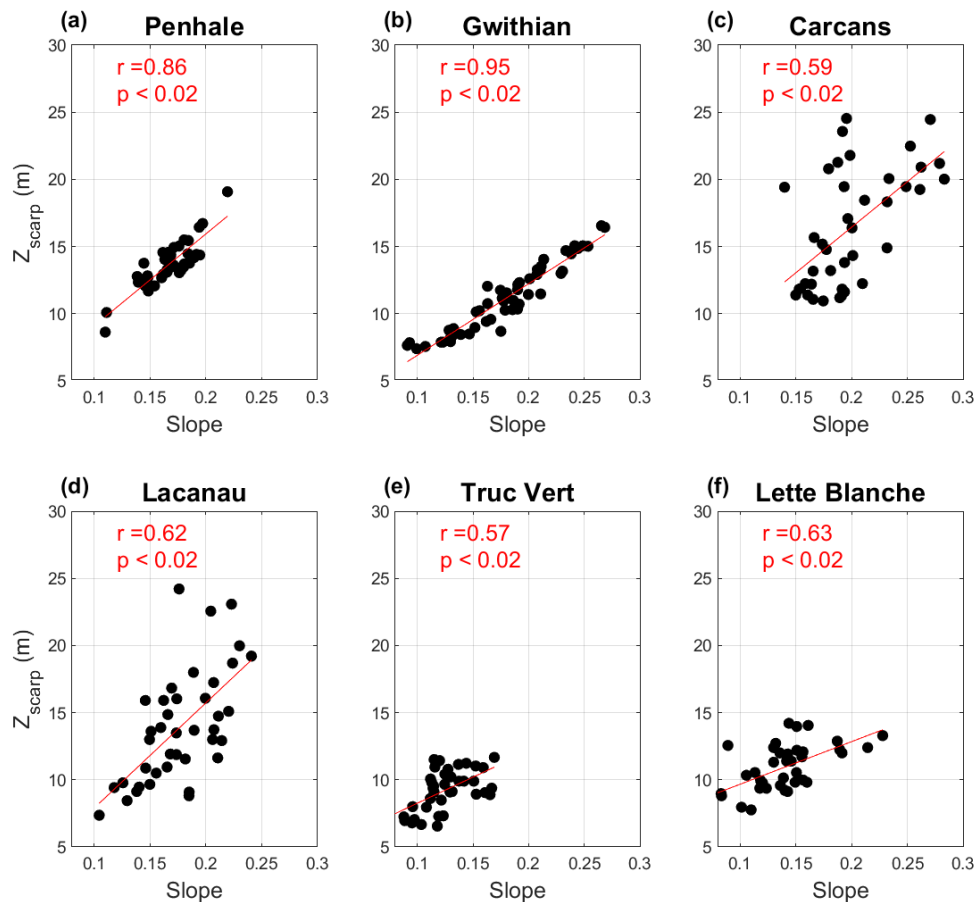


Figure 9. Post-storm dune scarping height,  $Z_{scarp}$ , in comparison to the pre-2014 dune slope,  $Slope$ , derived from 40 cross-shore profiles at six of the eight study sites where dune scarping without dune crest erosion was observed. The Pearson correlation coefficient,  $r$ , are added to assess the statistical significance of these relationships.

### 3.3. Morphological recovery of coastal dunes from extreme storms

#### 3.3.1. Dune profile recovery patterns from extreme storms

Representative pre-2014, post-storm and last survey (2020) cross-shore dune profiles were selected at the eight study sites to show and compare the morphological response to, and recovery from, extreme storms (Fig. 10). The 2020 dune profile at FBY shows that the dune continued to retreat over the subsequent years of the 2013/14 winter (Fig. 10a), highlighting the absence of recovery at this study site which is characterized severe chronic erosion ( $R = -2.1$  m/year). At PNH and GWI, limited recovery can be observed along the 2020 profiles in comparison of the 2014 ones, and is mainly restricted to the foot and the lower part of the dune face (Fig. 10b and c). NDM dune fully recovered, the dune face topography in 2020 is similar to the pre-2014 one, and accretion can be observed at the dune foot when comparing both profiles (Fig. 10d). The dune faces of CAR and LAC continued to retreat and to steepen between 2014 and 2020 within the megacusp embayments, with recovery at the dune foot, while little changes were observed throughout near the megacusp horns (Fig. 10e and f). An increase of the dune crest along with the steepening and retreat of these dunes can also be observed between 2011 and 2020, especially at LAC (Fig. 10f). The dune crest also rose by a couple of meters along several profiles of the TCV dune (Fig. 10g), and recovery of the dune face was larger compare to CAR and LAC. Full recovery can be observed at LBL dune along with accretion at the dune crest and behind (Fig. 10h).

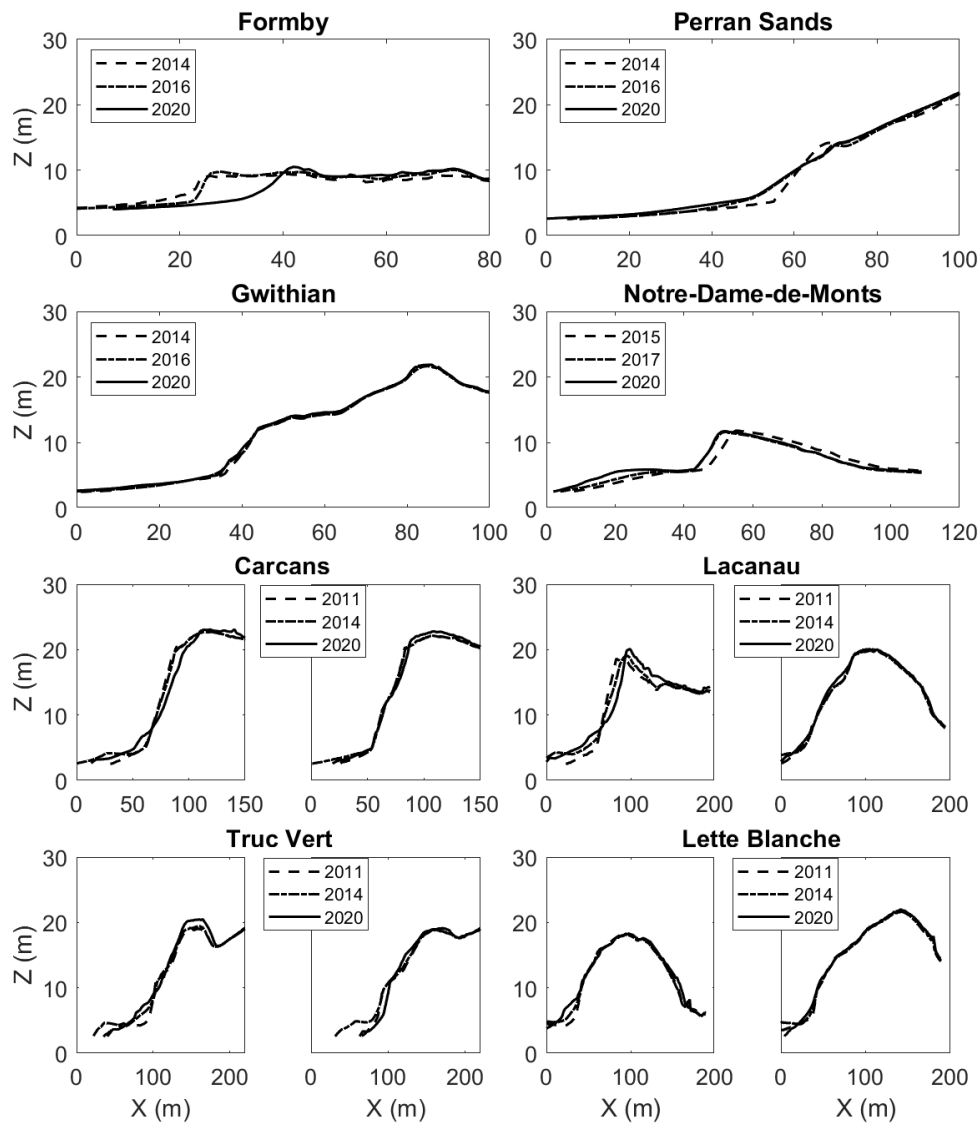


Figure 10. Representative pre-2014, post-storm and last survey (2020) cross-shore dune profiles extracted from LiDAR data at the eight study sites.

Alongshore-averaged sand volumes at the dune foot ( $\overline{dV_{\text{foot}}}$ ), the dune face ( $\overline{dV_{\text{face}}}$ ) and the dune top ( $\overline{dV_{\text{top}}}$ ) were used to have an overview of the vertical distribution of the recovered volumes of sand at each study site (Fig. 11). Results show that before the 2018/19 winter, dune foot volumes were fully recovered at all study sites except for FBY (Fig. 11a and b). The time-series of dune foot volumes

also show a regional coherent behavior along the SW coast of France (CAR, LAC, TCV and LBL), where strong similarities of the erosion/accretion pattern and magnitude at the dune foot are observed. These results differ from the time-series of the volume changes at the dune face (Fig. 11c and d), the volumes of sand lost during the 2013/14 winter were only fully recovered at NDM, TCV and LBL (Fig. 11c and d). The dune faces of PNH, GWI, CAR and LAC show limited to moderate recovery (11%, 63%, 19 % and 34%, respectively), even before the 2018/19 winter. Volume changes at the top of the dune shows erosion ( $-29 \text{ m}^3/\text{m}$ ) at FBY, limited accretion at PNH, GWI and NDM (1, 12 and  $13 \text{ m}^3/\text{m}$ , respectively), and relatively strong accretion at the Aquitanian sites (from 33 to  $110 \text{ m}^3/\text{m}$ ).

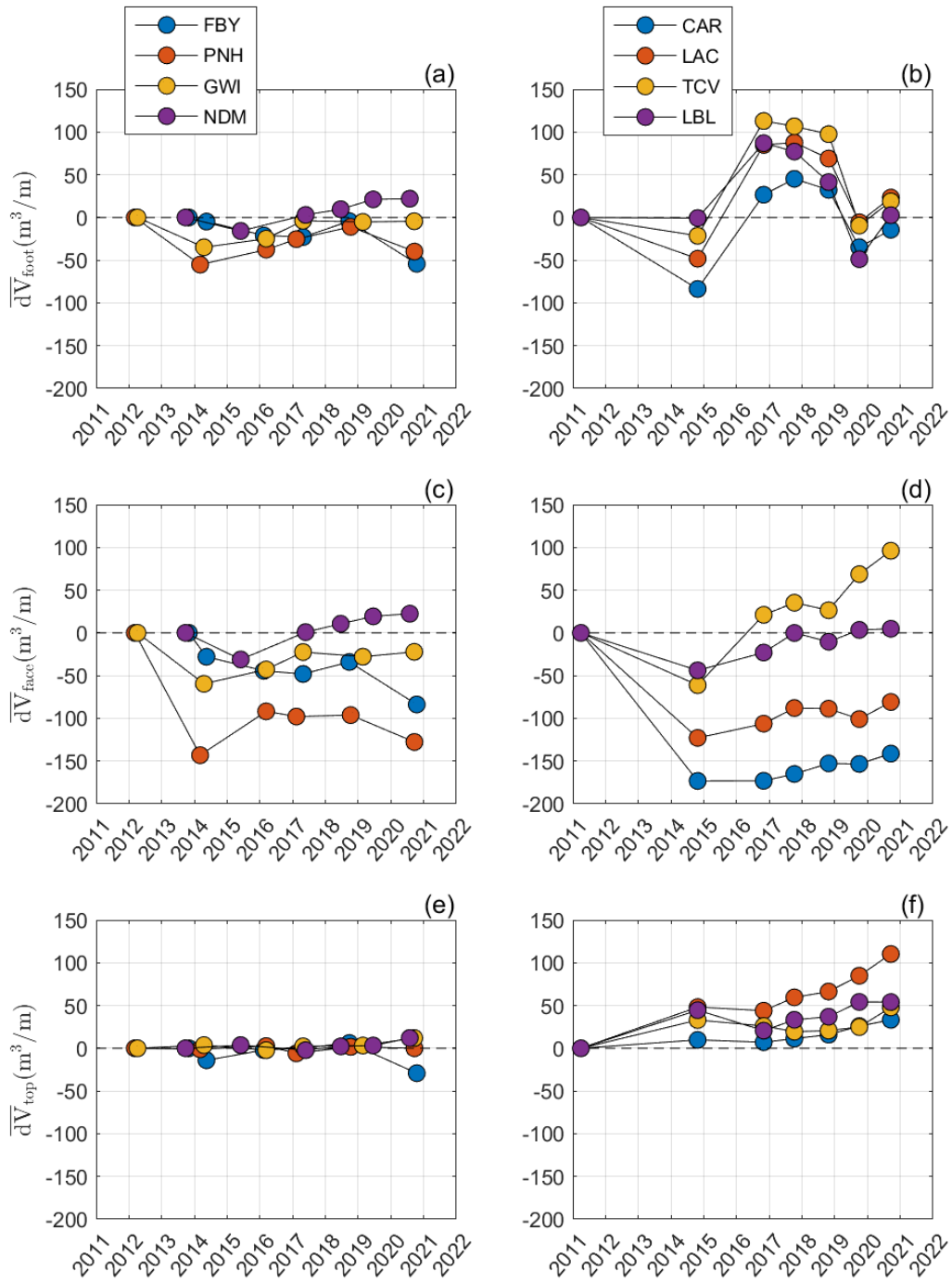


Figure 11. Time-series of the alongshore-averaged volume changes at the dune foot ( $\overline{dV_{\text{foot}}}$ ), the dune face ( $\overline{dV_{\text{face}}}$ ) and the top of the dune ( $\overline{dV_{\text{top}}}$ ) from 2011 to 2020 at the eight study sites.

### 3.3.2. Alongshore variability in dune recovery from extreme storms

PNH and LAC were selected as two contrasting examples of storm response, the difference of post-storm and 2020 DEMs were used to investigate here the spatial distribution of the recovered volumes of sand (Fig. 12). Relatively alongshore-uniform recovery can be observed at PNH, except for a stretch of 450 m at the middle of the dune that shows no recovery and further erosion (Fig. 12b). At LAC, the megacusp embayments formed during the 2013/14 winter remained the most dynamic areas of the dune over the 6 subsequent years. Within these megacusp embayments, accretion can be observed at the dune foot, while the dune face rolled over itself with the presence of symmetric and landward patterns of erosion/accretion (Fig. 12d).

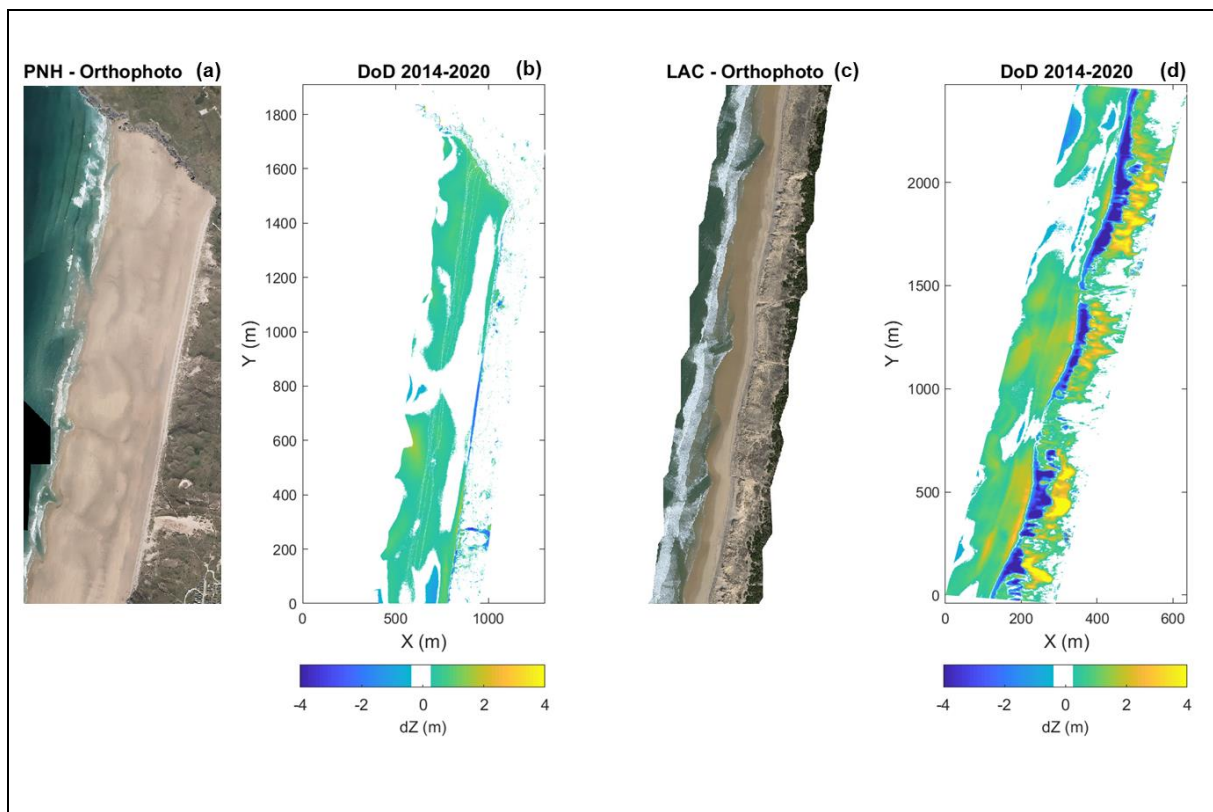


Figure 12. Orthophotos (a and c) and difference of post-storm (2014) and 2020 LiDAR DEMs (b and d) showing two contrasting examples of dune recovery from extreme storms at Penahle (PNH) and Lacanau (LAC).

Alongshore profiles of cross-shore volume changes over the stormy period ( $dV_{storm}$ ) and the 2014-2020 recovery period ( $dV_{recovery}$ ) are used to compare the alongshore variability in storm response and recovery for all study sites except for FBY dune where no recovery was observed (Fig. 13). At PNH, GWI, and NDM, both  $dV_{storm}$  and  $dV_{recovery}$  profiles are symmetric and alongshore uniform apart from blowouts at PNH ( $Y = 307$  m) and GWI ( $Y = 844$  m), and the stretch of dune that did not recover at PNH (from  $Y = 670$  to  $940$  m). Similarly, clear symmetric patterns of erosion and accretion that are not uniform alongshore and correspond to the megacusps described in the previous sections can be observed on the CAR, LAC, TCV and LBL. The length and magnitude of these patterns vary between the study sites and within the same study site (from 100 to 1000 m, and from 50 to 450 m<sup>3</sup>/m). Areas of accretion can be observed along the  $dV_{storm}$  profiles while the same areas show erosion during the recovery period, especially at LBL, suggesting that the whole stretch of dune is realigning. Although the magnitude of the recovery is correlated to the magnitude of the storm response at a dune scale, this result cannot be extrapolating when comparing the different study sites because dune that lost the largest volume of sand are not necessarily the ones that show the highest percentages of recovery ( $r = 0.36$ ).

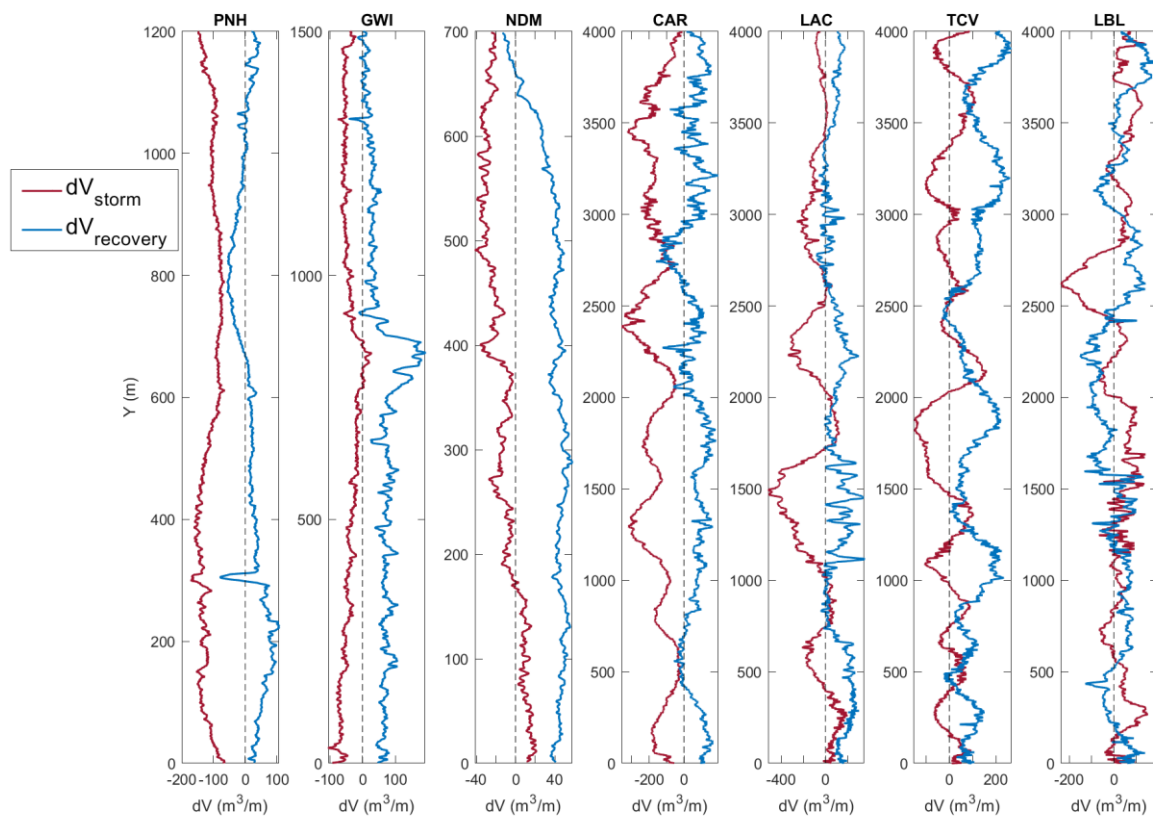


Figure 13. Alongshore profiles of cross-shore volume changes over the 2013/14 winter ( $dV_{storm}$ ) and the 2014-2020 recovery period ( $dV_{recovery}$ ) at all study sites except for FBY dune where no recovery was observed.

### 3.3.3. Controlling factor of dune recovery from extreme storms

Several morphological parameters were examined to explain the differences in recovery observed between the eight study sites. The best correlation ( $r = 0.81$ ,  $p\text{-value} = 0.01$ ) was found between the alongshore-averaged percentage of recovery,  $\overline{P_{recovery}}$  (%), expressed as the percentage of volume recovered between 2014 and 2020 in comparison to the volumes lost between the pre-2014 and 2014 surveys, and the multi-annual shoreline rate changes from 1984 to 2020,  $R$  (Fig. 14). This result suggests that dune recovery is mainly controlled by the local coastal sediment budget driving these

long-term trends. Other morphological parameters were tested against the alongshore-averaged percentage of recovery such as the dune slope and the volume of sand lost during the 2013/14 winter ( $\overline{dV_{storm}}$ ), but resulted in poor correlation ( $r = -0.44$  and  $r = 0.36$ , respectively).

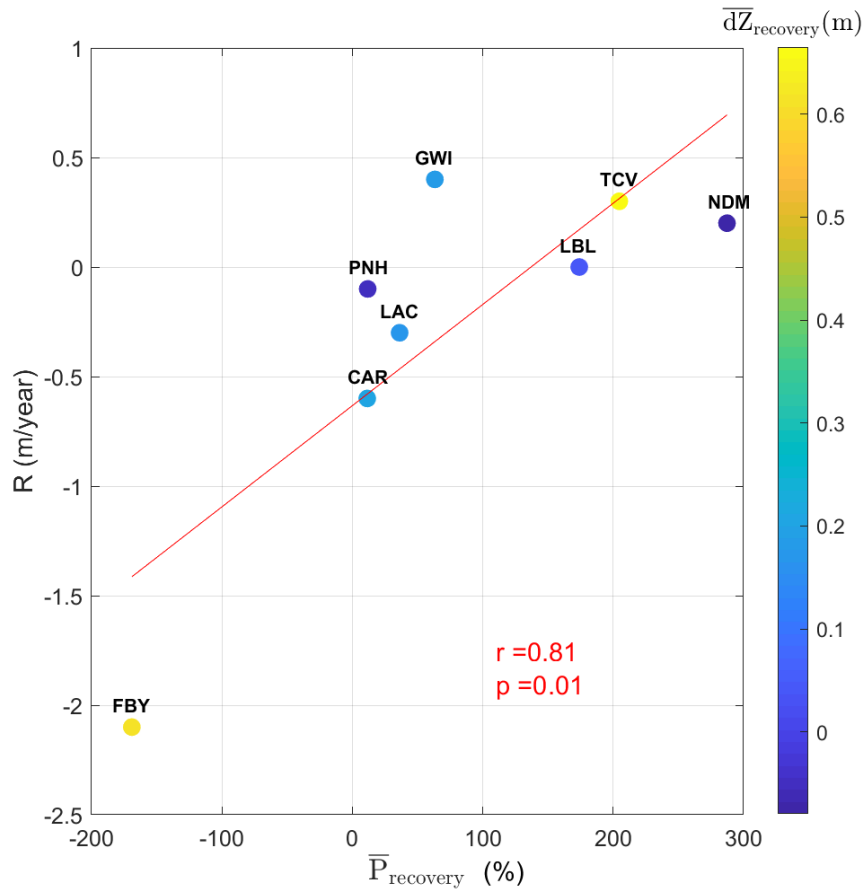


Figure 14. The alongshore-averaged percentage of volumes recovered between 2014 and 2020 in comparison to the volumes lost between the pre-2014 and the 2014 surveys,  $\overline{P}_{recovery}$ , against the alongshore-averaged shoreline rate changes from 1984 to 2020,  $R$ , at the eight study sites. The Pearson correlation coefficient,  $r$ , and the p-value of the Wilcoxon Rank-Sum test are added to assess the statistical significance of the relationship.

#### 4. Discussion

Several studies demonstrated that storm waves of the 2013/14 winter caused severe erosion at many coastal areas along the Atlantic coast of Europe (Blaise et al., 2015; Castelle et al., 2015; Masselink et al., 2016; Pye and Blott, 2016; Scott et al., 2016; Burvingt et al., 2018). This study shows that this winter was the first or second largest erosive event over the entire study period (2011-2020), at the eight coastal dunes distributed from the NW coast of England to the SW coast of France. At six of the eight study sites, storm response is characterized by severe dune scarping over the entire face of the dune, leading to large sand volume loss and dune foot retreat. For the dunes that are on average higher than 20 m, dune scarping height is generally limited to the face of the dune and does not exceed dune crest. In contrast, at FBY where the dune is lower than 15 m, the dune crest was eroded. At NDM, where the dune is even lower than FBY dune, storm response is characterized by a landward translation of the entire dune. These differences in dune profile response have an impact on the eroded volume of sand that were shown to be controlled by the dune face slope. This was also modelled on a 20 m high dune along the Dutch coast (De Winter et al., 2015), where severe dune scarping was observed. In comparison, modelled dune responses at 10 m high and relatively steep dunes along the Pacific Northwest coast of the United States showed that eroded volumes were instead correlated to the backshore beach slope (Cohn et al., 2019). The dune response at these sites did not show severe dune scarping, as observed here, but a relatively homogeneous vertical lowering along the upper part of the beach and lower part of the dune. This suggests that avalanching plays a significant role on the magnitude of eroded volumes at most of our sites, explaining the importance of the pre-storm dune slope. This contrasts with the dunes studied by Cohn et al. (2019) where swash excursions impacting the dune toe and controlled by the backshore beach slope had a key role on the storm response and eroded volumes. Another study (Itzkin et al., 2021) also demonstrated that low and wide dunes lose less sand volume than tall and narrow dunes during longer and more intense storms at beaches with similar width. This result can be verified here along the SW coast of France where beaches have similar characteristics, with CAR and LAC dunes losing more sand compared to TCV and LBL dunes.

The large spatial coverage of airborne LiDAR data used in this study also gave the opportunity to observe strong differences of the alongshore variability in storm response between the study sites. Along relatively wide, exposed and dissipative beaches, that can be found in NW and SW England (Burvingt et al., 2017), dunes show very little alongshore variability in storm response. The response of dunes along double-barred, strongly rip-channeled, beaches that can be found in SW France, inversely shows large alongshore variability that are highlighted by the presence of severe erosion hotspots with megacusp embayments which were shown to be controlled by the pre-winter outer-bar morphology (Castelle et al., 2015). An exception was observed at CAR dune where the contour of the megacusp embayments is less pronounced, CAR being the steepest dune of the eight study sites and lost the largest volumes of sand. Houser et al. (2013) showed that initial conditions and specifically the pre-storm variability of the crest elevation alongshore can control the impact of an extreme storm on 5 to 10 m high dunes along a barrier island (Santa Rosa Island, Florida, USA) . In our study, the crest elevation is too high, except at FBY and NDM, to play a major role in dune response to storms. Our results also suggest that alongshore variability in dune response can either be mainly controlled by the pre-storm topography of the dune and its slope (PNH and GWI), or by a complex combination of both topographic and bathymetric controls (CAR, LAC, TCV and LBL). Cohn et al. (2021) also showed that the alongshore variability of dune response to storms at 10 m high dunes (Outer Banks, North Carolina, USA) can be controlled by the presence of a deep nearshore bathymetric feature, the pre-storm beach and dune topography.

The analysis of the morphological evolution of the eight coastal dunes over the six years following the 2013/14 winter showed that dune recovery strongly varies between the study sites. Like other studies that examined beach and dune recovery (Houser et al., 2015; Scott et al., 2016; Castelle et al., 2017a; Dodet et al., 2018; Burvingt et al., 2018), our study shows that full recovery of the dunes from a sequence of extreme storms can take a couple of years (NDM, TCV, LBL), more than a decade (PNH, GWI, LAC) or never occur (FBY, CAR). When post-storm recovery takes place over several years, the inter-annual variability in winter wave conditions over these years control beach and dune recovery

(Burvingt et al., 2018; Dodet et al., 2018). Here, although the 2018/2019 winter did not stand out with regard to significant wave height, dune recovery was interrupted at all study sites, suggesting widespread storm waves associated with high water levels all across our study area. Dune foot volume were fully recovered or exceeded the volume that was lost during the 2013/14 winter at all study sites before the 2018/2019 winter, suggesting that conditions for recovery were met and recovery was initiated at all study sites. However, volumes of the dune face never returned or exceeded to their pre-2014 levels at most of the study sites (FBY, PNH, GWI, CAR, LAC) during the same six years. Like other studies which showed a regional coherent behaviour between beaches exposed to similar wave conditions (Bracs et al., 2016; Burvingt et al., 2018; Wiggins et al., 2019b), time-series of the dune foot volumes shows a regional coherency along the SW coast of France, suggesting a strong control of the wave climate on the recovery processes along this section of the dunes. Different types of morphological changes associated with recovery were observed that can be either described as relatively static where dune tend to return to its pre-2014 position and shape, or dynamic, where the dune is translating and reshaped while recovering the volume of sand lost during the extreme storms. At PNH, GWI and LBL, the overall position and profile of the dune have not changed and the dune has already returned (LBL) or is building back to its pre-2014 shape (PNH and GWI). This behavior suggests that these dunes are gradually returning to an equilibrium profile (Suanez et al., 2012; Houser et al., 2015; Robin et al., 2020). At LAC and TCV, dune recovery appears much more dynamic and is characterized by a landwards and upwards translation of the dune profile, that can be described as dune roll-over, also observed at other dunes with varying size and shapes (Brooks et al., 2017, Masselink et al., 2022)

Large variations in the magnitude of recovered sand volume were observed among the eight study sites. A recent study along the SW coast of England showed that the magnitude of intertidal beach volume recovered was well correlated with the storm erosion volume (Konstantinou et al., 2021). This result was verified here within each dune system where storm-driven erosion was strongly non-uniform alongshore, with accretion patterns mirroring erosion patterns (see Fig. 13). However, it was

not verified when making the comparison between the different study sites, since the dunes that lost the largest volumes of sand did not show the highest percentages of recovery. Instead, percentages of recovery were well correlated to the long-term shoreline changes from 1984 to 2021 ( $R$ ), suggesting a key role of coastal sediment budget on the ability of coastal dune systems to recover from severe storms. Although comparison between dune recovery magnitude and patterns, and long-term shoreline changes, and thus local sediment budget, are relatively scarce in the literature, this is in line with recent studies showing that a lack of sediment delivery back to the beach, and hence to the dune between storm events, results in the inability for dune recovery or translation (Davidson et al., 2021), and that lowest values of dune accumulation are associated with areas where the shoreline chronically retreats (Costas et al., 2020). In contrast, along semi-enclosed coastal systems and thus relatively constant sediment budget ( $R \approx 0$ ) such as embayed beaches, full recovery is usually reached with recovery time increasing with increasing storm intensity (Dodet et al. 2018; Konstantinou et al., 2021). It could also be considered that study sites characterized by chronic erosion have the steepest slope and thus lose larger volumes of sediment during storms that slow recovery but no correlation was found between dune face slope and long-term shoreline change rate.

Despite dune foot retreat and large dune face volume losses over the study period, continuous dune crest elevation increase and accretion at the upper part of the dune, defined as 'dune roll-over' (Masselink et al., 2022), was observed at the four sites along the SW coast of France. The largest increase in dune crest elevation occurred during the 2013/14 winter, supporting that optimal conditions for dune growth occur during storm events associated with strong winds but not necessarily at zones of shoreline progradation (Cohn et al., 2018; Coastas et al., 2020). The rate of dune crest elevation increase (from 4.2 to 12 cm/year) along the SW coast of France largely exceeds sea level rise rate of  $3.3 \pm 0.7$  mm/year at TCV over the past decade (D'Anna et al., 2021), alike the findings of van IJzendoorn et al. (2021), who showed that sea level rise outpaced by vertical dune toe translation during recent decades on prograding coastal areas along the Dutch coast. This supports the conclusion that transgression distances due to sea level rise are small in comparison to characteristic shoreline

excursions driven by storm events and subsequent reconstruction phases (Davidson-Arnott and Bauer, 2021). Extreme storms were also shown to have a positive contribution to the nearshore sediment budget by exchanging sediment between the lower and upper shoreface (Harley et al., 2022). Similar exchange occurs in the upper profile between beach and dunes during these extreme events, the relatively large quantity of sand stored within dunes is redistributed to the intertidal area and thus mitigate shoreline erosion. Although both sea-level rise and enhanced storminess are expected to accelerate dune retreat (Masselink et al., 2022), this analysis shows that coastal dunes can be resilient systems against extreme storms. Such beach-dune systems can adapt to sea level rise when sediment budget is not a limiting factor, suggesting that beaches and dunes can thus survive sea level rise pending accommodation space (Cooper et al., 2020). Vegetation cover is a controlling factor of dune morphodynamics (Durán and Moore, 2013; Ruggiero et al., 2018; Ruessink et al., 2019) and likely played a role in sediment transport during these strong wind conditions but could not be considered here due to the lack of in-situ data.

## 5. Conclusions

- The same morphological parameters, derived from nine years of airborne LiDAR topographic data at eight coastal dunes spread along the Atlantic coast of England and France, allowed a robust comparison of the spatial and temporal coastal dune morphological changes.
- Although coastal dune response to and recovery from an extreme winter shows a wide range of patterns and trajectories, key morphological controlling factors were also unraveled. We found that dune face slope and long-term shoreline change rates, characterizing local sediment budget, largely control eroded sand volume and percentage of recovery, respectively.
- Alongshore variability in storm-driven response is enforced by a site-specific combination of pre-storm offshore bathymetric and dune topographic alongshore variabilities, which can also have an impact on the patterns of recovery.

- Given that some of the coastal dunes were found to rise at a rate larger than sea-level rise, developing and maintaining consistent coastal monitoring programs at regional scale is crucial to better understand, model and manage coastal dunes.

## **Acknowledgments**

This work was supported by the European Commission with the Horizon 2020 Framework Programme (H2020) and Marie Skłodowska-Curie Actions (H2020-MSCA-IF-891807). Airborne LiDAR datasets collected along the coastline of NW and SW England (FBY, PNH and GWI) were commissioned by the Environment Agency (EA) and are freely available at <https://environment.data.gov.uk/> and <http://www.channelcoast.org/southwest/>. The same datasets were collected along the Vendée coast (NDM) by a consortium of observatories (OSUNA and OR2C) that are funded by the region Pays de la Loire and by the DREAL Pays de la Loire, and are freely available at <https://ids.osuna.univ-nantes.fr/>. Airborne LiDAR campaigns along the entire Aquitanian coast were commissioned by the Observatoire de la Côte de Nouvelle-Aquitaine (OCNA).

## **References**

- Aagaard, T., Davidson-Arnott, R., Greenwood, B., Nielsen, J., 2004. Sediment supply from shoreface to dunes: linking sediment transport measurements and long-term morphological evolution. *Geomorphology* 60, 205 – 224.
- Almar, R., Castelle B., Ruessink, B.G., Sénéchal, N., Bonneton, P., Marieu, V., 2009. High-frequency video observation of two nearby double-barred beaches under high-energy wave forcing. *Journal of Coastal Research* 56, 1706 – 1710.
- Autret, R., Dodet, G., Fichaut, B., Suanez, S., David, L., Leckler, F., Ardhuin, F., Ammann, J., Grandjean, P., Lallemand, P., Philipot, J.F., 2016. A comprehensive hydro-geomorphic study of cliff-top storm deposits on Banneg Island during winter 2013–2014. *Marine Geology* 382, 37–55.

Bauer, B.O., Hesp, P.A., Smyth, T.A.G., Walker, I.J., Davidson-Arnott, R.G.D., Pickart, A., Grilliot, M., Rader A., 2022. Air flow and sediment transport dynamics on a foredune with contrasting vegetation cover. *Earth Surface Processes Landforms* 47 (11), 2811-2829.

Blaise, E., Suanez, S., Stéphan, P., Fichaut, B., David, L., Cuq, V., Autret, R., Houron, J., Rouan, M., Floc'h, F., Ardhuin, F., Cancouët, R., Davidson, R., Costa, S., Delacourt, C., 2015. Bilan des tempêtes de l'hiver 2013–2014 sur la dynamique du recul du trait de côte en Bretagne. *Geomorphologie Relief Processus Environnement* 21, 267–292.

Bossard, V., Nicolae Lerma, A., 2020. Geomorphologic characteristics and evolution of managed dunes on the South West Coast of France. *Geomorphology* 367, 107312.

Bracs, M.A., Turner, I.L., Splinter, K.D., Short, A.D., Mortlock, T.R., 2016. Synchronised patterns of erosion and deposition observed at two beaches. *Marine Geology* 380, 196–204.

Brooks, S.M., Spencer, T., Christie, E.K., 2017. Storm impacts and shoreline recovery: mechanisms and controls in the southern North Sea. *Geomorphology* 283, 48–60.

Brown, J.M., Souza, A.J., Wolf, J., 2010. An investigation of recent decadal-scale storm events in the eastern Irish sea. *Journal of Geophysical Research* 115, C05018.

Burvingt, O., Masselink, G., Russell, P., Scott, T., 2017. Classification of beach response to extreme storms. *Geomorphology* 295, 722–737.

Burvingt, O., Masselink, G., Scott, T., Davidson, M., Russell, P., 2018. Climate forcing of regionally-coherent extreme storm impact and recovery on embayed beaches. *Marine Geology* 401, 112–128.

Butel, R., Dupuis, H., Bonneton, P., 2002. Spatial variability of wave conditions on the French Atlantic coast using in-situ data. *Journal of Coastal Research* 36, 96–108.

Castelle, B., Bonneton, P., Dupuis, H., Sénéchal, N., 2007. Double bar beach dynamics on the high-energy meso-macrotidal French Aquitanian Coast: A review. *Marine Geology* 245, 141 – 159

Castelle, B., Marieu, V., Bujan, S., Splinter, K.D., Robinet, A., Senechal, N., Ferreira, S., 2015. Impact of the winter 2013–2014 series of severe Western Europe storms on a double-barred sandy coast: Beach and dune erosion and megacusps embayments. *Geomorphology* 238, 135–148.

Castelle, B., Bujan, S., Ferreira, S., Dodet, G., 2017a. Foredune morphological changes and beach recovery from the extreme 2013/2014 winter at a high-energy sandy coast. *Marine Geology* 385, 41–55.

Castelle, B., Dodet, G., Masselink, G., Scott, T., 2017b. A new climate index controlling winter wave activity along the Atlantic coast of Europe: the West Europe pressure Anomaly. *Geophysical Research Letters* 44, 1384–1392.

Castelle, B., Ritz, A., Marieu, V., Nicolae Lerma, A., Vandenhove, M., 2022. Primary drivers of multidecadal spatial and temporal patterns of shoreline change derived from optical satellite imagery. *Geomorphology*, 413, 108360.

Cohn N., Ruggiero P., de Vries S., Kaminsky G.M., 2018. New Insights on Coastal Foredune Growth: The Relative Contributions of Marine and Aeolian Processes. *Geophysical Research Letters* 45 (10), 4965-4973.

Cohn, N., Ruggiero, P., García-Medina, G., Anderson, D., Serafin, K.A., Biel, R., 2019. Environmental and morphologic controls on wave-induced dune response. *Geomorphology* 329, 108-128.

Cohn, N., Brodie, K.L., Johnson, B., Palmsten, M.L., 2021. Hotspot dune erosion on an intermediate beach. *Coastal Engineering* 170, 103998.

Cooper, J. A.G., Masselink, G., Coco, G., Short, A.D., Castelle, B., Rogers, K., Anthony, E., Green, A.N., Kelley, J.T., Pilkey, O.H., Jackson, D.W.T., 2020. Sandy beaches can survive sea-level rise. *Nature Climate Change*, 10 (11), 993-995.

Costas, S., De Sousa, L.B., Kombiadou, K., Ferreira, O., Plomaritis, T.A., 2020. Exploring foredune growth capacity in a coarse sandy beach. *Geomorphology* 371, 107435.

D'Anna, M., Castelle, B., Idier, D., Rohmer, J., Le Cozannet, G., Thieblemont, R., Bricheno, L., 2021. Uncertainties in Shoreline Projections to 2100 at Truc Vert Beach (France): Role of Sea-Level Rise and Equilibrium Model Assumptions. *JGR Earth Surface* 126 (8), e2021JF006160.

Davidson, S.G., Hesp, P., Da Silva, G.M., 2021. Rapid shoreline erosion and dunefield Change, Salmon Hole, South Australia. *Science of the Total Environment* 767, 145406.

Davidson-Arnott, R.G.D., Bauer, B.O., 2021. Controls on the geomorphic response of beach-dune systems to water level rise. *Journal of Great Lakes Research* 47, 1594–1612.

Delgado-Fernandez, I., Davidson-Arnott, R., 2011. Meso-scale aeolian sediment input to coastal dunes: The nature of aeolian transport events. *Geomorphology* 126 (1–2), 217-232.

De Winter, R.C., Gongriep, F., Ruessink, B.G., 2015. Observations and modeling of alongshore variability in dune erosion at Egmond aan Zee, the Netherlands. *Coastal Engineering* 99, 167-175.

Dissanayake, P., Brown, J., Wisse, P., Karunarathna, H., 2015. Effects of storm clustering on beach/dune evolution. *Marine Geology* 370, 63–75.

Dodet, G., Castelle, B., Masselink, G., Scott, T., Davidson, M., Floc'h, F., Jackson, D., Suanez, S., 2019. Beach recovery from extreme storm activity during the 2013-14 winter along Atlantic coast of Europe. *Earth Surface Processes and Landforms* 44, 393-401.

Durán, O., Moore, L., 2013. Vegetation controls on the maximum size of coastal dunes. *Proc. Natl. Acad. Sci. USA* 110, 17217–17222.

Harley, M.D., Masselink, G., Ruiz de Alegría-Arzaburu, A., Valiente, N.G., Scott, T., 2022. Single extreme storm sequence can offset decades of shoreline retreat projected to result from sea-level rise. *Communications Earth & Environment* 3, 112.

Hesp, P.A., Walker, I.J., Chapman, C., Davidson-Arnott, R., Bauer, B.O., 2013. Aeolian dynamics over a coastal foredune, Prince Edward Island, Canada. *Earth Surface Processes Landforms* 38 (13), 1566-1575.

Houser, C., 2013. Alongshore variation in the morphology of coastal dunes: Implications for storm response. *Geomorphology* 199, 48-61.

Houser, C., Wernette, P., Rentschlar, E., Jones, H., Hammond, B., Trimble, S., 2015. Post storm beach and dune recovery: implications for barrier island resilience. *Geomorphology* 234, 54–63.

Itzkin, M., Moore, L.J., Ruggiero P., Hacker, S.D., Biel, R.G., 2021. The relative influence of dune aspect ratio and beach width on dune erosion as a function of storm duration and surge level. *Earth Surface Dynamics* 9, 1223–1237.

Konstantinou, A., Stokes, C., Masselink, G., Scott, T., 2021. The extreme 2013/14 winter storms: Regional patterns in multi-annual beach recovery. *Geomorphology* 389, 107828.

Launeau, P., Giraud, M., Ba, A., Moussaoui, S., Robin, M., Debaine, F., Lague, D., Le Menn, E., 2018. Full-Waveform LiDAR Pixel Analysis for Low-Growing Vegetation Mapping of Coastal Foredunes in Western France. *Remote Sensing* 10, 669.

Le Mauff, B., Juigner, M., Ba, A., Robin, M., Launeau, P., Fattal, P., 2018. Coastal monitoring solutions of the geomorphological response of beach-dune systems using multi-temporal LiDAR datasets (Vendée coast, France). *Geomorphology* 304, 121–140.

Lozano, I., Devoy, R.J.N., May, W., Andersen, U., 2004. Storminess and vulnerability along the Atlantic coastlines of Europe: analysis of storm records and of a greenhouse gases induced climate scenario. *Marine Geology* 210, 205–225.

Masselink, G., Scott, T., Davidson, M., Russell, P., Conley, D., 2015. The extreme 2013/2014 winter storms: hydrodynamic forcing and coastal response along the southwest coast of England. *Earth Surface Processes Landforms* 41, 378–391.

Masselink, G., Castelle, B., Scott, T., Dodet, G., Suarez, S., Jackson, D., Floc'h, F., 2016. Extreme wave activity during 2013/2014 winter and morphological impacts along the Atlantic coast of Europe. *Geophysical Research Letters* 43, 2135–2143.

Masselink G., Brooks, S., Poate, T., Stokes, C., Scott, T., 2022. Coastal dune dynamics in embayed settings with sea-level rise – Examples from the exposed and macrotidal north coast of SW England. *Marine Geology* 450, 106853.

Nicolae Lerma, A., Ayache, B., Ulvoas, B., Paris, F., Bernon, N., Bulteau, T., Mallet, C., 2019. Pluriannual beach-dune evolutions at regional scale: Erosion and recovery sequences analysis along the Aquitaine coast based on airborne LiDAR data. *Continental Shelf Research* 189, 10397.

Nicolae Lerma, A., Castelle, B., Marieu, V., Robinet, A., Bulteau, T., Bernon, N., Mallet, C., 2022. Decadal beach-dune profile monitoring along a 230-km high-energy sandy coast: Aquitaine, southwest France. *Applied Geography* 139, 102645.

Phillips, M.S., Harley, M.D., Turner, I.L., Splinter, K.D., Cox, R.J., 2017. Shoreline recovery on wave-dominated sandy coastlines: the role of sandbar morphodynamics and nearshore wave parameters. *Marine Geology* 385, 146–159.

Poate, T., Kingston, K., Masselink, G., Russell P., 2009. Response of high-energy, macrotidal beaches to seasonal changes in wave conditions: examples from North Cornwall, UK. *Journal of Coastal Research* SI 56.

Pye, K., Blott, S.J., 2016. Assessment of beach and dune erosion and accretion using LiDAR: impact of the stormy 2013–14 winter and longer term trends on the Sefton Coast, UK. *Geomorphology* 266, 146–167.

Robin, N., Billy, J., Castelle, B., Hesp, P., Laporte-Fauret, Q., Nicolae Lerma, A., Marieu, V., Rosebery, D., Bujan, S., Destribats, B., Michalet., 2020. Beach-dune recovery from the extreme 2013-2014 storms erosion at Truc Vert Beach, Southwest France: New insights from ground-penetrating radar. *Journal of Coastal Research*, SI 95, 588–592.

Robin, N., Billy, J., Castelle, B., Hesp, P., Nicolae Lerma, A., Laporte-Fauret, Q., Marieu, V., Rosebery, D., Bujan, S., Destribats, B., Michalet, R., 2021. 150 years of foredune initiation and evolution driven by human and natural processes. *Geomorphology* 374, 107516.

Ruessink, B.G., Schwarz, C.S., Price, T.D., Donker, J.J.A., 2019. A multi-year data set of beach-foredune topography and environmental forcing conditions at Egmond aan Zee, the Netherlands. *Data* 2019, 4(2), 73.

Ruggiero, P., Hacker, S., Seabloom, E., Zarnetske, P., 2018. The Role of Vegetation in Determining Dune Morphology, Exposure to Sea-Level Rise, and Storm-Induced Coastal Hazards: A U.S. Pacific Northwest Perspective. In: Moore, L., Murray, A. (eds) *Barrier Dynamics and Response to Changing Climate*. Springer, Cham.

Sallenger, A.H.J., Krabill, W., Swift, R., Brock, J., 2001. Quantifying hurricane-induced coastal changes using topographic lidar. *Coastal Dynamics '01 Proceedings*. American Society of Civil Engineers, Reston, Virginia, USA, 1007–1016.

De Vries, S., Southgate H.N., Kanning, W., Ranasinghe, R., 2012. Dune behavior and aeolian transport on decadal timescales. *Coastal Engineering* 67, 41-53.

Scott, T., Masselink, G., Russell, P., 2011. Morphodynamic characteristics and classification of beaches in England and Wales. *Marine Geology* 286, 1–20.

Scott, T., Masselink, G., O'hare, T., Saulter, A., Poate, T., Russell, P., Davidson, M., Conley, D., 2016. The extreme 2013/2014 winter storms: beach recovery along the southwest coast of England. *Marine Geology* 382, 224–241.

Splinter, K.D., Strauss, D.R., Tomlinson, R.B., 2011. Assessment of post-storm recovery of beaches using video imaging techniques: a case study at Gold Coast, Australia. *IEEE Transactions on Geoscience and Remote Sensing* 49 (12), 4704–4716.

Suanez, S., Cariolet, J.M., Cancouët, R., Ardhuin, F., Delacourt, C., 2012. Dune recovery after storm erosion on a high-energy beach: Vougot Beach, Brittany (France). *Geomorphology* 139-140, 16–33.

Valiente, N.G., Masselink, G., Scott, T., Conley, D., McCarroll, R.J., 2019. Role of waves and tides on depth of closure and potential for headland bypassing. *Marine Geology* 407, 60–75.

Valiente, N.G., Masselink, G., McCarroll, R.J., Scott, T., Conley, D., King, E., 2020. Nearshore sediment pathways and potential sediment budgets in embayed settings over a multi-annual timescale. *Marine Geology* 427, 106270. Van IJzendoorn, C.O., de Vries, S., Hallin, C., Hesp, P.A., 2021. Sea level rise outpaced by vertical dune toe translation on prograding coasts. *Scientific Reports* 11, 12792.

Vos, K., Splinter, K.D., Harley, M.D., Simmons, J.A., Turner, I.L., 2019. CoastSat: a Google Earth Engine-enabled Python toolkit to extract shorelines from publicly available satellite imagery. *Environmental Modelling and Software* 122, 104528.

Walker, I.J., Davidson-Arnott, R.G.D., Bauer, B.O., Hesp, P.A., Delgado-Fernandez, I., Ollerhead, J., Smyth, T.A.G., 2017. Scale-dependent perspectives on the geomorphology and evolution of beach-dune systems. *Earth-Science Reviews* 171, 220-253.

Wernette, P., Thompson, S., Eyler, R., Taylor, H., Taube, C., Medlin, A., Decuir, C., Houser, C., 2018. Defining Dunes: Evaluating How Dune Feature Definitions Affect Dune Interpretations from Remote Sensing. *Journal of Coastal Research* 34 (6), 1460-1470.

Wiggins M., Scott, T., Masselink, G., Russell, P., McCarroll, R.J., 2019a. Coastal embayment rotation: Response to extreme events and climate control, using full embayment surveys. *Geomorphology* 327, 385-403.

Wiggins, M., Scott, T., Masselink, G., Russell, P., Valiente, N.G., 2019b. Regionally-Coherent Embayment Rotation: Behavioural Response to Bi-Directional Waves and Atmospheric Forcing. *Journal of Marine Science and Engineering* 7 (4), 116.